

The following publication Lin, X., Zeng, L., & Wu, M. (2024). Integrating single atoms with nanoparticle catalysts for efficient electrochemical energy conversion [10.1039/D4TA02585G]. *Journal of Materials Chemistry A*, 12(29), 17793-17816 is available at <https://doi.org/10.1039/D4TA02585G>.

Journal of Materials Chemistry A

Materials for energy and sustainability

Accepted Manuscript

This article can be cited before page numbers have been issued, to do this please use: X. Lin, L. Zeng and M. Wu, *J. Mater. Chem. A*, 2024, DOI: 10.1039/D4TA02585G.



This is an Accepted Manuscript, which has been through the Royal Society of Chemistry peer review process and has been accepted for publication.

Accepted Manuscripts are published online shortly after acceptance, before technical editing, formatting and proof reading. Using this free service, authors can make their results available to the community, in citable form, before we publish the edited article. We will replace this Accepted Manuscript with the edited and formatted Advance Article as soon as it is available.

You can find more information about Accepted Manuscripts in the [Information for Authors](#).

Please note that technical editing may introduce minor changes to the text and/or graphics, which may alter content. The journal's standard [Terms & Conditions](#) and the [Ethical guidelines](#) still apply. In no event shall the Royal Society of Chemistry be held responsible for any errors or omissions in this Accepted Manuscript or any consequences arising from the use of any information it contains.

Integrating Single Atoms with Nanoparticles Catalysts for Efficient Electrochemical Energy Conversion

View Article Online
DOI: 10.1039/D4TA02585G

Xiaorong Lin^a, Lin Zeng^{b,*}, Maochun Wu^{a,*}

^aDepartment of Mechanical Engineering, The Hong Kong Polytechnic University,
Hung Hom, Kowloon, Hong Kong, 999077, China

^bDepartment of Mechanical and Energy Engineering, Southern University of Science
and Technology, Shenzhen 518055, China

Corresponding authors: E-mail: zengl3@sustech.edu.cn (L. Zeng);
maochun.wu@polyu.edu.hk (M.C. Wu)

Abstract:

Advances in various clean energy conversion and storage technologies (e.g., fuel cells, water electrolysis, and metal-air batteries) requires catalysts that are highly active, selective, and stable. Single-atom catalysts, with their unique structure, high atom utilization and well-defined active sites, have gained considerable attention in electrocatalysis. However, their practical applications are hindered by low metal loading and too single active sites. Integrating single atoms with nanoparticles (including clusters) into a single catalytic entity (SA/NPCs) has been demonstrated to be an effective way to overcome these challenges by synergizing different active species, thus leading to considerably enhanced catalytic performance. This review aims to provide a systematic summary of recent advances in this emerging field. First, we classify the integrated effects that contribute to the enhanced activity, selectivity, and stability of SA/NPCs into electron transfer effect, tandem effect, and parallel effect. Then, the realization and synthetic challenges of SA/NPCs are discussed based on two types of substrates, i.e., carbon- and metal-based carriers. Furthermore, we summarize and elaborate state-of-the-art applications of these catalysts in various electrochemical

reactions, including oxygen reduction reaction, oxygen evolution reaction, hydrogen evolution reaction, and other emerging electrocatalytic reactions such as carbon dioxide and nitrogen reduction reactions. Finally, the challenges and opportunities associated with the development and implementation of this class of catalysts are highlighted to provide insights for future endeavors.

Keywords: Single atoms; nanoparticles; nanoclusters; electrocatalysts; electrochemical energy conversion

1. Introduction

The pressing concerns over environmental pollution, climate change, and energy crisis have triggered considerable efforts worldwide in developing sustainable electrochemical energy conversion technologies, such as fuel cells, water electrolyzers, and metal-air batteries ¹⁻⁵. These devices rely on various electrochemical reactions, such as oxygen reduction/evolution reactions (ORR/OER) and hydrogen evolution reactions (HER), to convert chemical energy into electrical energy, or vice versa. However, the kinetics of these reactions are sluggish, resulting in low efficiencies and poor performance of these devices ^{6, 7}. Therefore, catalysts that can enhance the rates of electrochemical conversion are essential to the success of these electrochemical technologies ⁸⁻¹¹. At present, the most widely used catalysts are typically made of precious metals (e.g., platinum ¹² and palladium ¹³) because of their exceptional catalytic activity. However, the scarcity and cost issues of noble metals pose significant hindrances for their widespread applications. Moreover, even precious metal catalysts present limited selectivity and stability for catalytic reactions ^{14, 15}. For example, as the most widely used catalyst for ORR, platinum is susceptible to corrosion and poisoning during prolonged operation, leading to decreased catalytic activity ¹⁶. Additionally, poor selectivity in the reaction can lead to the formation of harmful byproducts (e.g.,

hydrogen peroxide)¹⁷, which compromises the efficiency and longevity of electrochemical devices. Hence, the development of advanced electrocatalysts with low cost and high activity, selectivity, as well as stability is of paramount importance.

To this end, a wide variety of catalysts have been reported, among which metal-based catalysts dominate due to their diverse electronic structures and chemical properties¹⁸⁻²¹. The catalytic performance of metal-based catalysts can be tailored by adjusting particle size, chemical composition, active site valence, and atomic coordination of catalysts²²⁻²⁶. Remarkably, downsizing the particle size to nanoscale has been found to profoundly change the catalytic behavior of metal-based catalysts. Thanks to the advances in nanotechnology, the past several decades have witnessed a boom in electrocatalysis using nanostructured metal catalysts for various electrochemical reactions^{27,28}. The dramatic changes in catalytic performance brought about by nanomaterials can be summarized as follows. (1) Smaller particles display a larger surface area, thus increasing the number of active sites available for catalytic reactions and ultimately enhancing performance²⁹⁻³³. (2) The modification of electronic structures resulting from size reduction can promote charge transfer and facilitate the desired reaction steps, thereby improving catalytic efficiency and accelerating overall reaction kinetics³⁴⁻³⁷. (3) Variation in nanoparticle size affects the production of various reaction intermediates, thus impacting the selectivity of the final product^{38,39}. The unique advantages of nanoparticle catalysts in electrocatalytic reactions can also be exemplified by their surface/interface^{40,41}, crystal facets^{42,43}, morphology⁴⁴⁻⁴⁶, and other properties⁴⁷. By carefully regulating these properties, it is possible to design and optimize nanoparticle catalysts with superior performance for various electrochemical reactions.

Despite extensive studies of nanoparticle catalysts, their broader application is

hindered by their relatively large size and the fact that only surface atoms are active in catalysis⁴⁸⁻⁵⁰. To remove this limitation and maximize metal utilization, researchers have proposed to create active sites at atomic level, termed “single-atom catalysts (SACs)”. The term “SACs” was introduced by Zhang et al. in 2011, when they successfully synthesized Pt-based SACs by loading Pt atoms onto the Fe₂O₃ surface and demonstrated their excellent activity in CO oxidation⁵¹. Since then, researchers have designed various types of SACs to achieve high catalytic efficiency in different reactions. The advantages of SACs can be summarized in the following three aspects. First, SACs have highly distributed active sites at atomic level, allowing maximum metal utilization efficiency (up to 100%) and maximizing atomic economy^{52,53}. Second, the uniformity of active sites and geometric structures of SACs ensure that reactant molecules interact uniformly across the catalyst surface, mitigating side reactions caused by variations in active sites and thus effectively improving catalytic selectivity^{54,55}. Third, the homogeneous structure of SACs is more conducive to characterization and recognition, which is instrumental in investigating the structure-performance relationship of the catalysts at the atomic level and revealing the mechanism of catalytic reactions⁵⁶. However, the ultra-small size and high surface energy of SACs can lead to stability problem⁵⁷. Additionally, the single active site and low metal loading of SACs^{20, 58-60} make them inferior to catalyze reactions that involve multiple steps⁶¹.

In recent years, considerable efforts have been directed at addressing the limitations of SACs by combining them with heterogenous nanoparticles (including clusters). The integration of these two components in one catalyst offers several unique advantages, which are highlighted as follows. (1) Synergistic enhancement of catalytic activity and selectivity. The introduced nanoparticles can regulate the electron configuration of neighboring single atoms, leading to optimized adsorption energy of

the reaction intermediates, thus promoting reaction kinetics⁶²⁻⁷⁰. Moreover, the optimization of intermediate adsorption energy can also catalyze the specific reaction pathways, driving the reaction toward the desired direction and thus boosting the selectivity⁷¹⁻⁷³. (2) Enhanced active sites. By introducing both single atoms and nanoparticles, the number and variety of active sites can be increased, which is of great significance for catalyzing multi-step electrocatalytic reactions in tandem or promoting different types of electrocatalytic reactions through parallel effect⁷⁴⁻⁷⁹. (3) Improved stability. The electron interaction between the SACs and nanoparticles helps to stabilize the electronic structure of the single atoms, thereby avoiding agglomeration or deactivation during the catalytic reactions^{80, 81}. Through this ingenious combination, numerous catalysts with exceptional catalytic performance have been developed, showing great promise for developing highly effective catalysts^{70, 82-84}. However, there is a lack of comprehensive review of this rapidly emerging class of catalysts. In this review, we aim to provide a comprehensive summary of the development of SA/NPCs as illustrated in **Fig. 1**. We start with discussing the integrated effects within SA/NPCs, followed by categorizing the catalysts and summarizing their up-to-date applications in different electrocatalytic reactions. Finally, future research opportunities and perspectives in developing novel heterogeneous catalysts using this combining strategy are highlighted. We hope that the timely summary of state-of-the-art knowledge of this exciting field will attract more research interest and promote the development of catalysts for next-generation electrochemical energy conversion and storage.

View Article Online
DOI: 10.1039/D4TA02585G

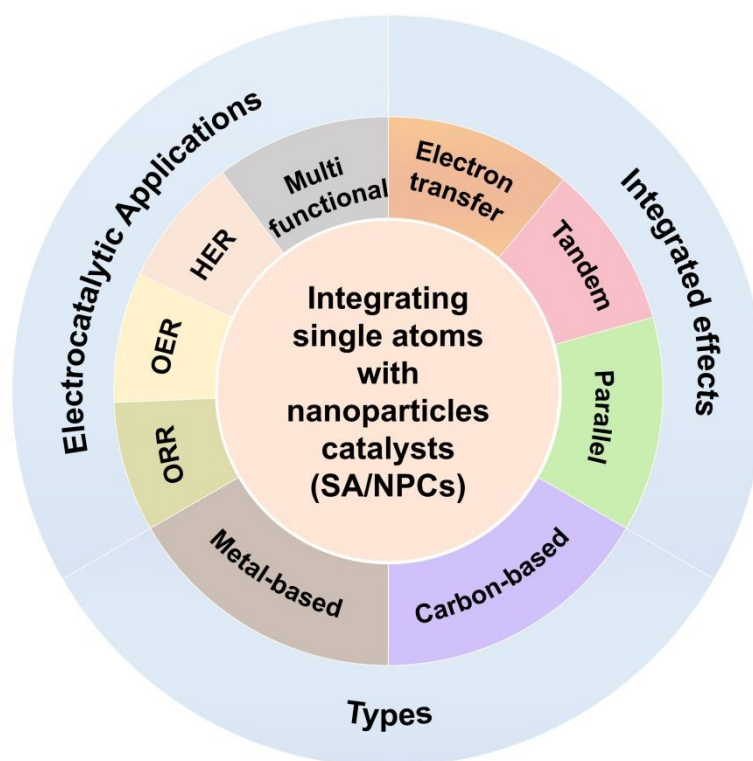


Fig. 1. Schematic diagram of the integrated effects, types, and electrocatalytic applications of SA/NPCs.

2. Integrated effects of SA/NPCs

The coexistence of single atoms and nanoparticles does not just increase the number of active sites but will improve the activity, selectivity, and stability of metal-based catalysts in a collective and/or synergetic way. An in-depth understanding of the cooperative functions of catalysts is essential to the establishment of a structure-performance relationship that will guide the design and optimization of highly efficient catalysts. Although the exact mechanisms underlying the cooperative behavior of active species in SA/NPCs remain unclear, it can usually be classified into the following three integrated effects: electron transfer effect, tandem effect, and parallel effect (**Fig. 2**). It is important to acknowledge that catalytic reactions often encompass multiple pathways/steps and involve numerous electron transfers. Furthermore, it is highly probable that several of the aforementioned effects may coexist in actual catalytic reactions, leading to a significant enhancement in catalytic performance. However, it

remains a formidable challenge to elucidate the underlying mechanisms linking the observed distribution of active sites to the resulting catalytic performance.

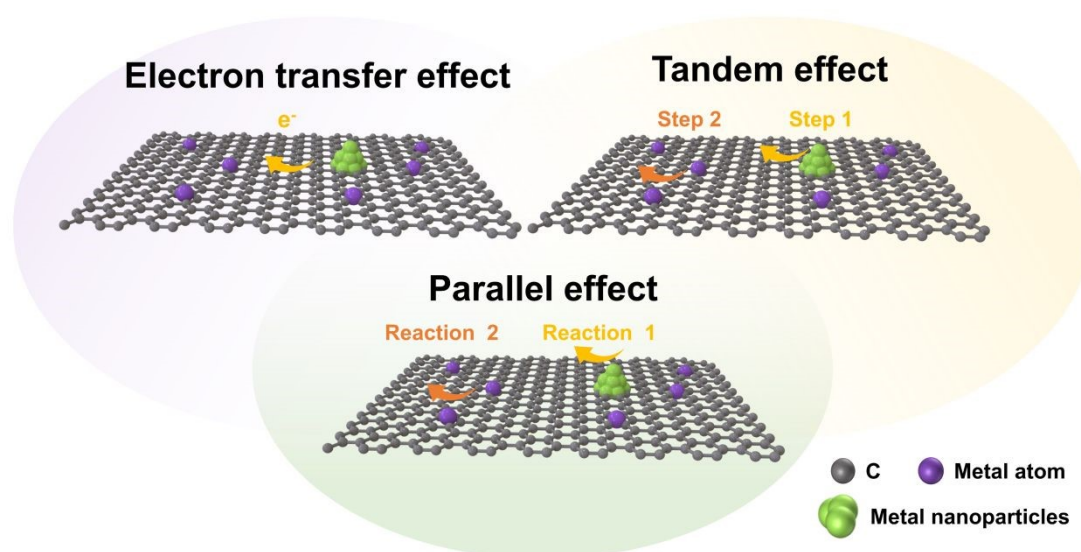


Fig. 2. Schematic diagram of the integrated effects of SA/NPCs. Electron transfer effect: There is an electron transfer between single atoms and nanoparticles, and the optimized electronic structure improves catalytic performance; Tandem effect: Single atoms and nanoparticles accelerate one or two specific steps in the reaction, thus collaboratively accelerating the entire reaction; Parallel effect: Single atoms and nanoparticles catalyze different reactions respectively and thus endows the catalysts with multifunctional properties.

2.1 Electron transfer effect

The efficient control of the electronic structure of catalysts has been recognized as an effective way to enhance electrocatalytic activity. Particularly, the electrochemical performance of single atom and nanoparticle catalysts is highly dependent on the electronic environment at atomic level⁸⁵. Noting that most SA/NPCs use carbon as support, the local electronic environment of the catalysts can be optimized by tuning the metal-carbon interaction. Researchers have found that the integration of single atoms with nanoparticles can synergistically alter the state of charge of active sites, which reduces the binding strength of reaction intermediates, lowers the reaction energy barrier, and optimizes the adsorption/desorption behavior, thereby considerably improving electrocatalytic performance. For example, Su et al. demonstrated that doping single metal atoms (e.g., Fe, Co, and Ni) in a carbon substrate could effectively

reshape the electronic structure of the supported Ru nanoparticles, resulting in an optimized electronic structure that enhanced electrocatalytic activity (**Fig. 3a**)⁸⁶. As shown in **Fig. 3b**, the strong interaction between Ru₅₅ and M₁@OG (oxygen-doped graphene) regulates their charge state. Specifically, the introduction of single metal atoms into oxygen-doped graphene leads to electron deficiencies in neighboring carbon atoms, resulting in greatly improved electron transfer from the Ru nanoparticles to the carbon substrate. Consequently, the relatively positive charge density at the Ru nanoparticle interface weakens the binding strength of the H* intermediates, thereby enhancing the catalytic activity toward HER (**Fig. 3c**). These results suggest that the remote electronic interaction of single atoms on carbon substrates with Ru nanoparticles can optimize the free adsorption energy of intermediates, thus achieving efficient HER electrocatalysis.

The unique carbon structure also plays a key role in regulating the electronic interaction between single atoms and nanoparticles. For example, Feng et al. constructed a Ru-based electrocatalyst structure featuring Ru nanoparticles as the core, wrapped by single-atom RuN_x species dispersed in a fullerene-like carbon cage as the shell (Ru_{NP}@RuN₄-FC, **Fig. 3d**)⁸⁷. Compared with the planar carbon matrix configuration (Ru_{NP}-RuN₄/PC), the electronic density of state (DOS) for Ru_{NP}@RuN₄-FC exhibits a lower d-band center (ϵ_d). Based on the d-band center theory, a decrease in ϵ_d value gives rise to weaker but more favorable bonding strength of hydrogen for hydrogen production (**Fig. 3e**). Additionally, Ru_{NP}@RuN₄-FC exhibits a much lower Gibbs free energy of hydrogen (ΔG_{H^*} , **Fig. 3f**), indicating the stronger hydrogen adsorption process. Bader charge analysis further revealed that the electron transfer from the inner Ru nanoparticles to the single-atomic Ru on Ru_{NP}@RuN₄-FC modulates the charge distribution of Ru single atoms, thereby promoting water

dissociation. Therefore, the electronic structure of $\text{Ru}_{\text{NP}}@\text{RuN}_4\text{-FC}$ was optimized due to the combination of Ru nanoparticles and single-atomic Ru decorated fullerene-like carbon shell, which consequently boosted the HER activity.

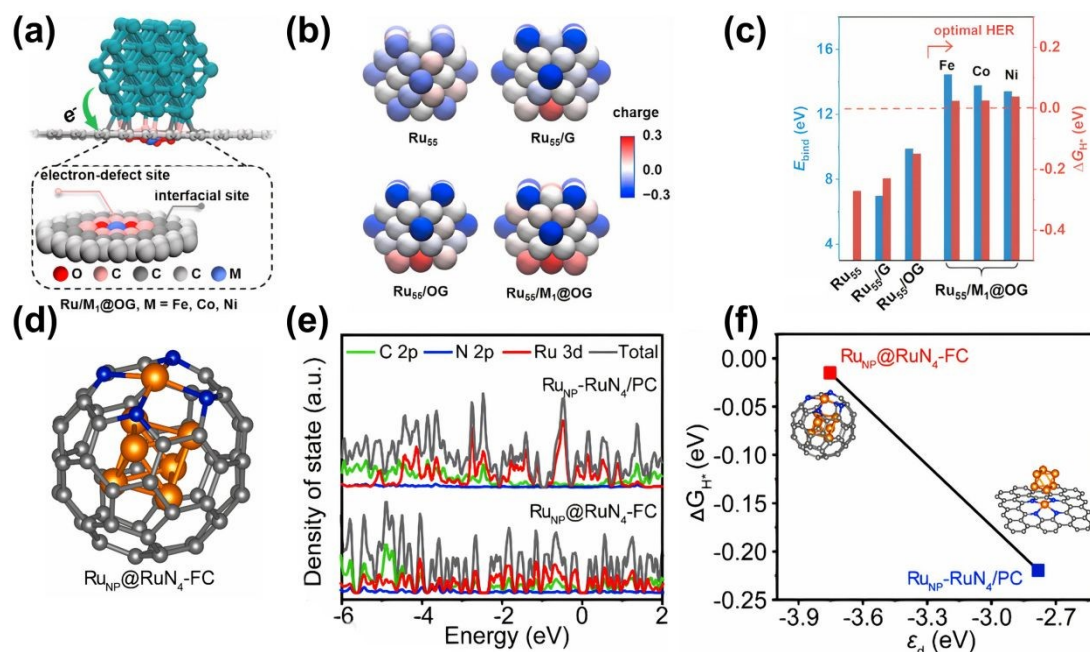


Fig. 3. (a) Theoretical model of Ru_{55} supported on O-doped graphene with dispersed metal atoms. (b) Bader charge analysis projected to Ru_{55} cluster. (c) Binding energies of $\text{Ru}_{55}/\text{M}_1@\text{OG}$ and freestanding Ru_{55} , and its corresponding ΔG_{H^*} . Reproduced from Ref. ⁸⁶, Copyright 2021 Wiley-VCH. (d) Structure of $\text{Ru}_{\text{NP}}@\text{RuN}_4\text{-FC}$. (e) Density of state diagram of $\text{Ru}_{\text{NP}}@\text{RuN}_4\text{-FC}$ and $\text{Ru}_{\text{NP}}\text{-RuN}_4/\text{PC}$. (f) Relationship of ΔG_{H^*} against the ϵ_d of the Ru atoms in $\text{Ru}_{\text{NP}}@\text{RuN}_4\text{-FC}$ and $\text{Ru}_{\text{NP}}\text{-RuN}_4/\text{PC}$. Reproduced from Ref. ⁸⁷, Copyright 2022 Elsevier.

2.2 Tandem effect

Electrocatalytic reactions, such as OER and HER, usually involve complex elementary reaction steps ^{88,89}. The introduction of both single atoms and nanoparticles into one catalyst has been shown to increase the variety of active sites, where each active site can accelerate one or two steps in the complex reactions and collectively accelerate the overall reaction. This catalytic process is commonly referred to as tandem or relay catalysis. A noteworthy example of tandem catalysis is demonstrated by Cao and colleagues, who successfully synthesized a highly efficient OER electrocatalyst containing dual active sites of Fe-NiOOH small particles and NiC₄ single atoms ⁹⁰.

From the free-energy paths of four-electron transfer during the OER process, the limiting step for Ni single atoms is $*OH \rightarrow *O$, while $*O \rightarrow *OOH$ for Fe-NiOOH (**Fig. 4a**). Cao et al. proposed that Ni SAs/Fe-NiOOH adopted a tandem catalysis process to achieve high OER activity, where Fe-NiOOH nanoparticles were responsible for the first two elementary reactions ($*OH$ and $*O$ formation) with a thermodynamically favorable pathway. The formed $*O$ then migrated to the surface of the NiC₄ single atoms, completing the subsequent conversion and desorption process (**Fig. 4b and c**). The tandem effect allowed Ni single atoms and Fe-NiOOH nanoparticles to collaboratively reduce the overall reaction energy barrier and promote the OER process. Similarly, the tandem effect has been observed to promote the HER process. For example, Zhang et al. reported the nickel oxide supported Ru single-atoms and nanoclusters catalyst (Ru_{SA+NC}/NiO-NF) for the typical multi-step alkaline HER⁹¹. For the HER in an alkaline medium, the overall pathway can be divided into H₂O-adsorption, H₂O-dissociation, and H-recombination. As shown in **Fig. 4d**, H₂O presents thermodynamically more favorable adsorption/dissociation on the Ru single-atoms sites than on Ru nanoclusters sites and NiO sites. Additionally, the Ru nanoclusters sites possess a more negative ΔG_{H^*} value, indicating the released H prefers to be absorbed on the Ru nanocluster sites (**Fig. 4e**). Owing to the weak binding energy between NiO and H, the adsorbed H migrates from the Ru nanocluster sites to NiO sites through H spillover and desorbs from NiO sites. Therefore, the tandem effect among multiple active sites (Ru single-atoms, Ru nanoclusters, and NiO) collectively catalyze the whole HER process (**Fig. 4f**).

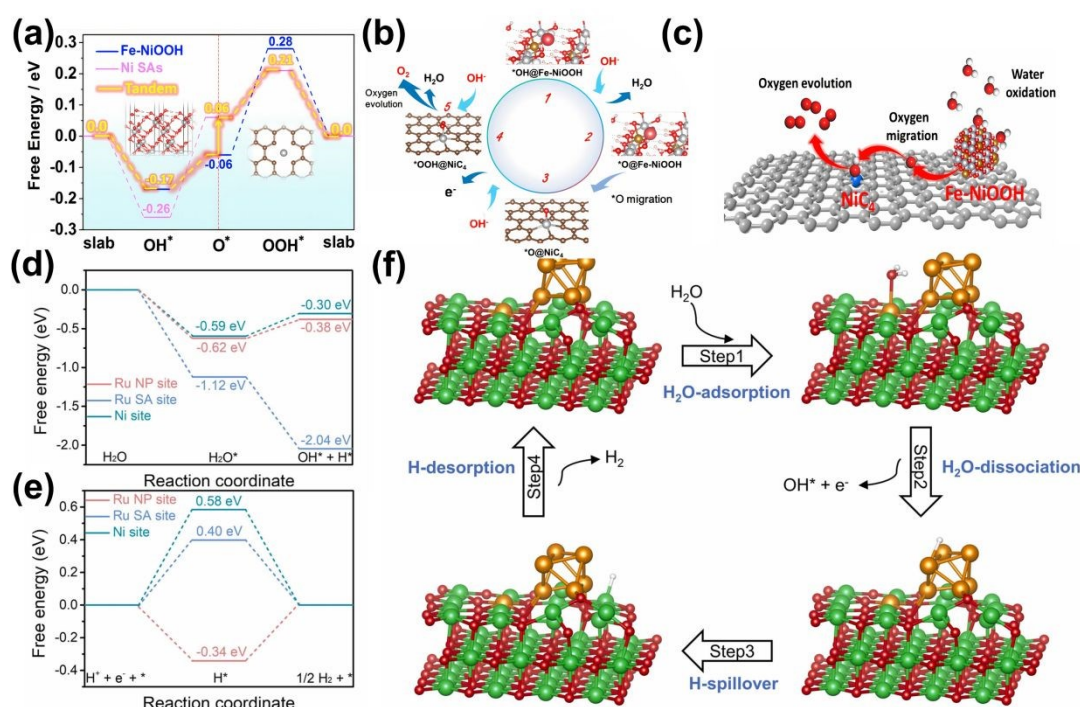


Fig. 4. (a) Free energies of intermediates on Ni-C₄ SAs and Fe-NiOOH. (b) The tandem catalysis mechanism of Ni SAs/Fe-NiOOH for OER. (c) Schematic diagram of OER through an oxygen migration mechanism. Reproduced from Ref. ⁹⁰, Copyright 2021 Elsevier. (d) The free energy diagrams of H₂O adsorption and H₂O-dissociation on different active sites. (e) The free energy diagrams of H-adsorption on different active sites. (f) Schematic illustration of the synergistic effect mechanism among Ru single-atom site, Ru nanocluster site, and NiO site during the alkaline HER process. Reproduced from Ref. ⁹¹, Copyright 2020 Elsevier.

2.3 Parallel effect

The combination of single atoms and nanoparticles can also catalyze different reactions at the same time to achieve multifunctional catalytic properties, which is classified as parallel effect ⁹². For example, Ding et al. proposed a carbon nanotube-bridging strategy to synthesize an ORR/OER bifunctional oxygen electrocatalyst enriched with highly active single-atom Fe sites and nanosized NiCo hydroxides for all-solid-state zinc-air batteries (ZABs, **Fig. 5a**) ⁹³. In this hybrid electrocatalyst, single-atom FeN₅ active sites promote the ORR, while nanosized NiCo hydroxides is responsible for catalyzing OER. This parallel effect was confirmed by in-situ Raman characterizations. As the applied potential shifts negatively from 0.97 to 0.17 V (**Fig.**

5b), the characteristic peaks at 591, 685, and 751 cm^{-1} exhibit a trend of attenuation and then enhancement, which suggest that oxygen-containing intermediates (e.g., $\ast\text{OOH}$, $\ast\text{O}$, and $\ast\text{OH}$) are generated on the Fe active centers. The further negative shift in the applied potential that resulted in relatively enhanced signals is possibly due to the desorption of the $\ast\text{OH}$ product. These results suggest that the ORR process occurred at the Fe active center, likely via the $\text{O}_2 \rightarrow \ast\text{OOH} \rightarrow \ast\text{O} \rightarrow \ast\text{OH} \rightarrow \text{OH}^-$ pathway. As for the OER reaction, with a further increase in applied potential, two distinct new peaks appear at 476 and 554 cm^{-1} , which were ascribed to the metal (Ni, Co)–O vibrations in (Ni, Co)–OOH ⁹⁴, suggesting that the real active site for OER should be the corresponding nanosized hydroxide (**Fig. 5c**). In addition to their bifunctional activity for ORR/OER, SA/NPCs can be endowed bifunctional activity in HER and OER for overall water splitting ⁹⁵. For example, Sun et al. synthesized a hybrid catalyst, Au-Fe₁NC/NF, containing Au nanoclusters and Fe single atoms, which exhibited outstanding alkaline HER and OER activity (**Fig. 5d**) ⁹⁶. Density functional theory (DFT) calculations revealed that the presence of Fe single atoms in Au-Fe₁NC/NF induces the electron delocalization of Au nanoclusters, thereby enhancing the HER activity. In-situ Raman experiments provided insight into the mechanism of synergy in OER. As the potential and time increased, the OER intermediate Fe₁–O–O–H was observed, demonstrating the effectiveness of Fe single atoms as active sites for OER (**Fig. 5e and f**). These findings highlighted the synergistic interaction between Au nanoclusters and Fe single atoms, leading to excellent performance in alkaline water splitting for the Au-Fe₁NC/NF catalyst.

SA/NPCs also show potential as trifunctional catalysts due to the parallel effect ⁹⁷, ⁹⁸. For example, Li et al. prepared hollow carbon nanotubes integrated with cobalt atoms with Co₉S₈ nanoparticles (CoSA + Co₉S₈/HCNT) ⁹⁸. Theoretical calculations

confirmed that the interaction between Co_9S_8 and single-atom CoN_4 sites optimize the electronic configuration of the active sites to synergistically lower the reaction barriers and facilitate the ORR, OER, and HER simultaneously (**Fig. 5g-i**). Ahn et al. developed a trifunctional catalyst for HER/ORR/OER by combining NiFe nanoclusters with atomically dispersed Ni active sites⁹². The authors proposed that strategically placing the metal clusters close to the surrounding single atom-based active sites greatly optimize the multifunctional catalytic activity. However, due to the diversity and complexity of active species, the reaction mechanism of such catalysts needs to be further explored.

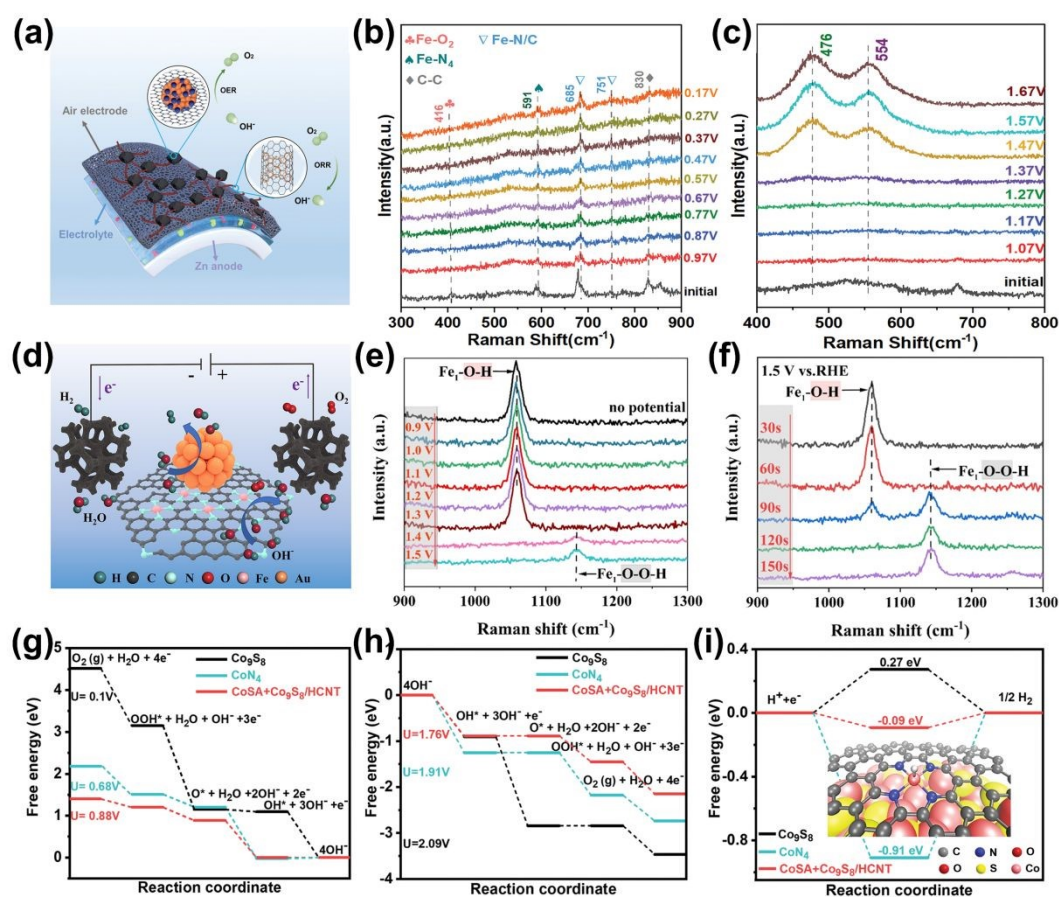


Fig. 5. (a) Schematic diagram of the all-solid-state Zn-air battery with a FePc||CNTs||NiCo/CP cathode. In situ Raman spectra collected on FePc||CNTs||NiCo/CP for (b) the ORR process and (c) the OER process. Reproduced from Ref.⁹³, Copyright 2022 Wiley-VCH. (d) Schematic illustration of overall water splitting on Au-Fe₁NC/NF. Alkaline OER in situ Raman spectra for Au-Fe₁NC with the increase of potential (e) and time (f). Reproduced from Ref.⁹⁶, Copyright 2023

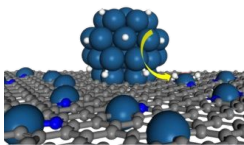
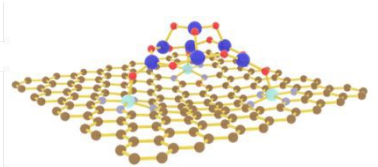
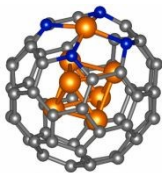
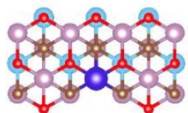
American Chemical Society. (g) Free energy diagrams for the thermodynamic limiting potentials of ORR steps. (h) Free energy diagrams for the thermodynamic limiting potentials of OER steps. (i) Free energy diagrams of Co₉S₈, CoN₄, and CoSA + Co₉S₈/HCNT for HER and inset is the model of adsorption configuration of HER on CoSA + Co₉S₈/HCNT. Reproduced from Ref. ⁹⁸, Copyright 2020 Wiley-VCH.

To sum up, the exceptional catalytic performance of SA/NPCs catalysts can be attributed to the electron transfer effect, tandem effect, and parallel effect. Electron transfer effect between single atoms and nanoparticles plays a crucial role in adjusting the adsorption strength of intermediates, reducing the Gibbs free energy, promoting reactant dissociation, and ultimately enhancing catalytic ability. The tandem effect observed in SA/NPCs involves the participation of both single atoms and nanoparticles in different intermediate steps of each catalytic reaction, leading to a collective acceleration of the overall reaction. Moreover, the parallel effect in SA/NPCs can facilitate various catalytic reactions or lower the energy barriers of different catalytic reactions through their interactions. These integrated effects in SA/NPCs provide tremendous opportunities for the rational design and development of highly efficient catalysts.

3. Categories and construction challenges of SA/NPCs

The catalytic activity, selectivity and stability of SA/NPCs are closely related to the catalyst structure. To gain a deeper understanding of the structure-performance relationship, the reported SA/NPCs catalysts are categorized into two types based on the substrates of catalysts. One type involves loading single atoms and nanoparticles onto the same carbon substrates ⁹⁹⁻¹⁰¹, while in the other type, metal nanoparticles serve directly as the substrate for the single atoms, with their stability ensured through strong chemical bonding ^{102, 103}. Typical structure models and features of each categories are summarized and compared in **Table 1**. In addition to the structural considerations, we will also discuss the key challenges in fabricating these SA/NPCs.

Table 1. Categories of SA/NPCs

Type	Structural model	Structural feature	Ref.
Anchoring	 PtSA/NC-DG Color code: Pt dark blue; C gray N blue; H white.	Co-loading of single atoms and nanoparticles on carbon carriers	Reproduced from Ref. ¹⁰⁴ , Copyright 2020 Chinese Chemical Society.
Anchoring	 Pt-ACs/CoNC Color code: C brown; N gray; O red; Co cyan-blue; Pt blue.	Anchoring nanoparticles onto single atom-doped carbon carriers	Reproduced from Ref. ¹⁰⁵ , Copyright 2022 Springer Nature.
Wrapping	 Ru _{NP} @RuN ₄ -FC Color code: Ru gold, N blue; C gray.	Wrapping nanoparticles with single atom-doped carbon	Reproduced from Ref. ⁸⁷ , Copyright 2022 Elsevier.
Metal nanoparticles-based	 Mo ₂ TiC ₂ T _x -Pt _{SA} Color code: Pt darkblue; Mo pink; O red. Ti light blue; C brown.	Doping single atoms into nanoparticles	Reproduced from Ref. ¹⁰⁶ , Copyright 2018 Nature.

3.1 Carbon-based SA/NPCs

Single atoms and nanoparticles co-loaded onto the carbon matrix are the most widely studied SA/NPCs. Carbon materials usually possess abundant anchoring sites due to the inherent defects ¹⁰⁷ and surface functional groups ^{108, 109}, thus facilitating the

uniform deposition of metal single atoms and nanoparticles. Furthermore, heteroatom (e.g., nitrogen) doping of carbon matrix can further increase the deposition possibility¹¹⁰⁻¹¹². Based on the distribution relationship between metals and carbon carriers, carbon-based SA/NPCs can be further divided into two categories: anchoring type and wrapping type.

3.1.1 Anchoring type

The anchoring type refers to the direct anchoring of metals onto the carbon substrate materials, which generally can be divided into two scenarios. One is that the single atoms and nanoparticles bind to the substrate through metal–N or metal–O bonds^{113, 114}, where the two active species are spatially adjacent to each other but lack direct chemical bonds. In such catalysts, single atoms and nanoparticles tend to act as isolated active centers for different catalytic steps, resulting in enhanced catalytic performance through a tandem effect^{91, 104}. For example, Zhu et al. developed a catalyst consisting of Pt single atoms and nanoclusters on nitrogen-doped carbon substrates (PtSA/NC-DG, **Fig. 6a**) to promote electrocatalytic HER¹⁰⁴. They obtained nitrogen-doped defective graphene (DG) by pyrolyzing a physical mixture of glucose and carbon nitride. Subsequently, Pt single atoms were anchored to DG through a one-step chemical deposition, followed by a further thermal treatment to convert some Pt single atoms with unsaturated coordination structures into Pt nanoclusters. The coexistence of Pt single atoms and nanoclusters was confirmed by the high-angle annular dark-field scanning transmission electron microscope (HAADF-STEM) and the Fourier-transform extended X-ray absorption fine structure (FT-EXAFS) spectrum of PtSA/NC-DG, revealing Pt-C/N/O and Pt-Pt coordination (**Fig. 6b and c**). DFT calculations further revealed that Pt nanoclusters promote water dissociation into *H and *OH, while Pt single atoms facilitate the H-H coupling into gaseous hydrogen,

leading to a tandem catalytic hydrogen evolution process.

View Article Online
DOI: 10.1039/D4TA02585G

The second type involves the direct deposition of the nanoparticles on a single atom, which results in a strong chemical interaction between them. The synthesis strategy for this type of catalyst involves the gradual construction of both active constituents: single atoms and nanoparticles. To effectively anchor nanoparticles, single-atom sites often require specific properties. Previous research has demonstrated that the formation of metal-oxygen-metal chemical bonds or metal-metal quasi-covalent bonds can significantly enhance the stability of the catalyst structure. For instance, Zhao et al. utilized isolated Co atoms and nitrogen co-doped porous carbon (CoNC) as a unique substrate¹⁰⁵. The isolated Co atoms possess a positive charge and are stabilized by four surrounding N atoms in the equatorial plane, along with one O atom in the axial position. These O atoms above the Co single atoms can effectively capture Pt ions incorporated during the wet-impregnation process, resulting in the formation of stable Pt atomic clusters (Pt ACs) on the surface of the CoNC substrate (**Fig. 6d**). The HAADF-STEM image and the corresponding DFT optimized structure (**Fig. 6e**) provide evidence of the strong interaction between Pt and Co species due to the formation of Pt-O-Co coordination, which stably anchors the Pt ACs. FT-EXAFS spectra and DFT further demonstrated that the Pt ACs were composed of Pt-O-Pt units with a lower Pt oxidation state, which is beneficial for hydrogen generation (**Fig. 6f and g**). Guo and his colleagues initially used pyrolysis to prepare carbon supports containing single-atom Cr-N₄ sites (Cr-N-C)¹¹⁵. Subsequently, they successfully anchored Pt ACs on the Cr-N₄ sites through wet-impregnation and heat treatment processes (**Fig. 6h**). The combination of experimental studies and DFT calculations revealed that a strong Pt-Cr quasi-covalent bonding interaction is formed at the interface of Pt-ACs and Cr-N₄ sites via 3d-5d orbital hybridization (**Fig. 6i-k**). This

interaction effectively restricts the migration and aggregation of Pt atoms, leading to the immobilization/stabilization of Pt ACs, thereby significantly improving the durability of the catalyst. Moreover, the oxophilic unsaturated Cr-N₄ sites exhibit a favorable binding affinity towards OH_{ads} species, which enhances water dissociation and makes the catalyst highly active for alkaline HER catalysis.

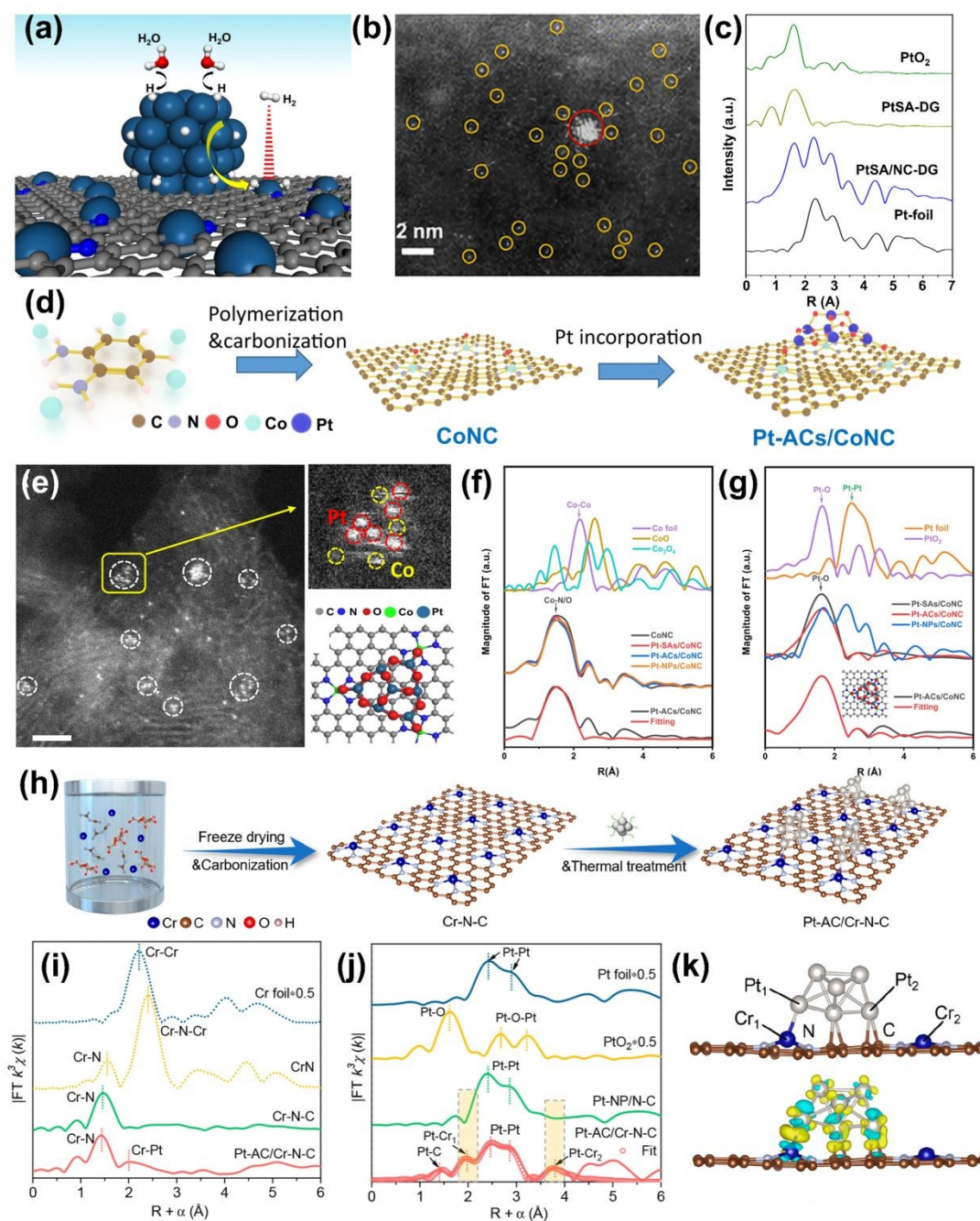


Fig. 6. (a) Proposed mechanism of the HER on PtSA/NC-DG. (b) HAADF-STEM image of PtSA/NC-DG. (c) FT-EXAFS spectra of PtSA/NC-DG and references. Reproduced from Ref. ¹⁰⁴, Copyright 2020 Chinese Chemical Society. (d) Schematic

illustration of the preparation of Pt-ACs/CoNC. (e) STEM images of Pt-ACs/CoNC and corresponding simulated image and DFT optimized structure. (f) The normalized X-ray absorption near-edge structure (XANES) spectra and the FT-EXAFS spectra at Co K-edge of CoNC, Pt-SAs/CoNC, Pt-ACs/CoNC, Pt-NPs/CoNC and references. EXAFS curves between the experimental data and the fit of Pt-ACs/CoNC at Co K-edge. (g) FE-EXAFS spectra derived from EXAFS of Pt foil, PtO₂, Pt-SAs/CoNC, Pt-ACs/CoNC and Pt-NPs/CoNC. EXAFS curves between the experimental data and the fit of Pt-ACs/CoNC. Inset is the fitted structure. Reproduced from Ref. ¹⁰⁵, Copyright 2022 Springer Nature. (h) Synthesis and structural characterizations of Pt-AC/Cr-N-C. (i) FE-EXAFS spectra at Cr K-edge. (j) FE- EXAFS spectra at Pt L₃-edge. (k) Atomic structure model of the Pt-AC/Cr-N-C catalysts. Reproduced from Ref. ¹¹⁵, Copyright 2023 American Chemical Society.

3.1.2 Wrapping type

The wrapping type pertains to the encapsulation of nanoparticles within a substrate material that contains single-atom sites. Unlike anchored metal nanoparticles that typically exhibit poor stability due to dissolution in adverse electrochemical environments, by wrapping the nanoparticles with a carbon network, a protective barrier is created so that direct exposure to corrosive electrolyte solutions is prevented ¹¹⁶⁻¹¹⁹. Additionally, the interaction between nanoparticles and single-atom doped carbon induces an electron-donating effect, leading to alteration in the charge density on the single-atom sites and thus enhancing the kinetics of electrocatalytic reactions ^{120, 121}. Consequently, the wrapping type of SA/NPCs exhibit high catalytic stability and activity simultaneously. For example, Zhao et al. developed a gaseous acid-mediated method to prepare Fe-N-C catalysts with stable isolated Fe-N-C sites (**Fig. 7a**) ¹²². Subsequently, secondary heat-treated and temperature control were employed to obtain graphene-encapsulated metallic Fe nanoparticles (as confirmed by annular bright-field (ABF)-STEM image in **Fig. 7b**). The Fe single atoms and nanoparticles co-exist catalyst (as confirmed FT-EXAFS spectra in **Fig. 7c**) exhibited excellent activity and stability for ORR. It was demonstrated that the enhanced performance resulted from the strong interaction between single-atom sites and adjacent Fe nanoparticles, which optimizes the electron structure of isolated Fe sites and reduces the energy barrier of

ORR rate-limiting steps.

View Article Online
DOI: 10.1039/D4TA02585G

However, further integration of different types of single atoms and nanoparticles into a single system can be challenging, often necessitating the development of sophisticated synthesis strategies. In a recent study, Wang et al. successfully synthesized a hybrid electrocatalyst, denoted as Ni SAs-Pd@NC, wherein Ni single atoms and sub-10 nm Pd nanocrystals were embedded in N-doped porous carbon frameworks¹²³. The combination of Ni single atoms and small-sized noble metal nanoparticles was seldom observed in reported literature, primarily attributed to the variation in synthetic approaches and thermal stability between single atoms and nanoparticles. To achieve this coexistence, the researchers employed a three-step process of “coordination- π - π stacking-anneal” based on the protection of 1-naphthylamine during pyrolysis. Initially, the planar Pd^{II}-(C₁₀H₇-NH₂) complex was formed through the coordination of Pd^{II} with 1-naphthylamine. Then, NiPc was added, and through π - π stacking interactions, NiPc@Pd^{II}-(C₁₀H₇-NH₂) complexes were formed. Finally, Ni^{II} restricted by macrocyclic molecules was reduced to Ni single atoms under 600 °C pyrolysis conditions (**Fig. 7d**). Meanwhile, Pd^{II} sites were reduced to Pd nanoparticles, and C₁₀H₇-NH₂ was converted to carbon frameworks, which encapsulated the Pd nanoparticles and supported the Ni single atoms, as confirmed by HRTEM and FT-EXAFS spectra in **Fig. 7e and f**, respectively. In this composite catalyst, the Ni single atoms provided active sites for OER, while the Pd nanoparticles promoted ORR activity, and the porous carbon framework enhanced diffusion/transfer kinetics and overall structural robustness. Consequently, Ni SAs-Pd@NC showed excellent electrocatalytic activity, with an ORR half-wave potential of 0.84 V, which was comparable to that of commercial Pd/C. In addition, it displayed an OER overpotential of 380 mV at 10 mA cm⁻², which closely approached that of RuO₂. It

should be noted that the interaction between the encapsulated nanoparticles and the single atoms loaded on the carbon carrier is a critical factor in enhancing the catalytic activity of wrapping type SA/NPCs. The synthesis conditions, such as synthesis temperature and ligand selection, can significantly influence the formation of this structure.

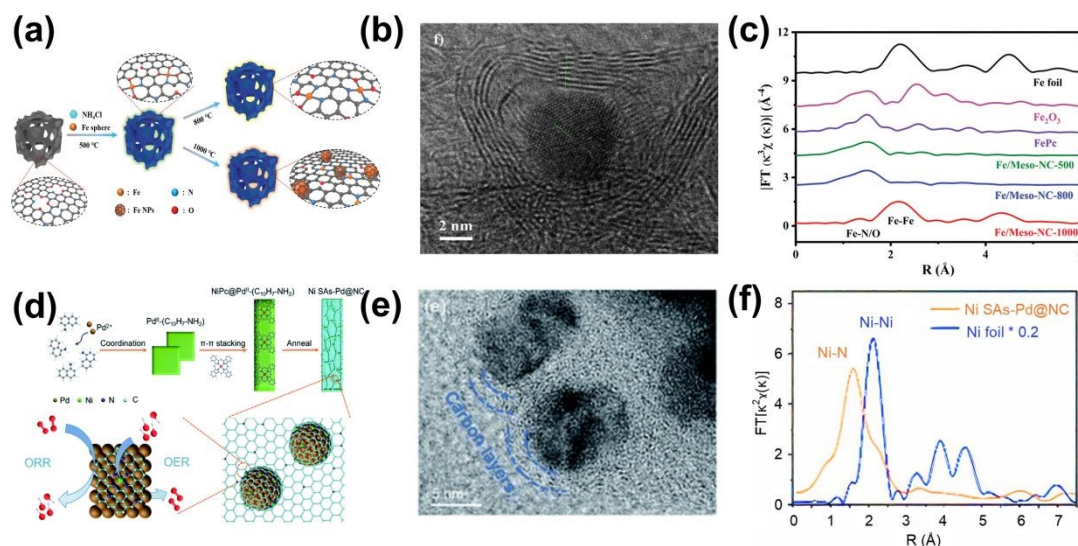


Fig. 7. (a) Illustration of the synthesis process of Fe/Meso-NC-T samples. (b) ABE-STEM image of Fe/Meso-NC-T. (c) FT-EXAFS spectra of the Fe K-edge. Reproduced from Ref. ¹²², Copyright 2021 Wiley-VCH. (d) Schematic illustration showing the formation pathway of Ni SAs-Pd@NC. (e) HRTEM image of Ni SAs-Pd@NC. (f) FT-EXAFS spectra of the Ni K-edge. Reproduced from Ref. ¹²³, Copyright 2022 Royal Society of Chemistry.

3.2 Metal nanoparticles-based SA/NPCs

In addition to carbon-based SA/NPCs, single atoms can be directly dispersed/doped onto/into the nanoparticles, forming metal nanoparticle-based SA/NPCs. In this category, nanoparticles can be classified into different types, including metal compounds (e.g., oxides ^{91, 124-128}, carbides ¹²⁹, nitrides ⁶³, sulfides ¹³⁰, and phosphides ^{131, 132}) and nanoalloys ¹³³⁻¹³⁵. By employing nanoparticles as a stable substrate, metal nanoparticle-based SA/NPCs offer excellent structural stability, thus significantly enhancing the long-term effectiveness of the prepared catalysts. Moreover, the strategic doping of single atoms onto metal nanoparticles presents numerous

advantages, not only in terms of synthesis methods but also the profound effects these doped single atoms exert on the adjustment of the metal nanoparticles' surface structure and electronic configuration. Consequently, a remarkable reduction in the activation energy required for catalytic reactions is achieved, thereby achieving highly efficient catalytic activity^{136, 137}. Currently, there are two main methods used to construct catalysts with this type of structure. The first method involves introducing single atoms during the growth process of nanocrystals by means of co-reaction with low doses of single-atom sources. For example, Liu et al. synthesized atomically dispersed Ir atoms incorporated into a spinel Co_3O_4 lattice through a solvothermal method (**Fig. 8a**)¹²⁴. Energy-dispersive X-ray spectroscopy (EDS) elemental mapping in **Fig. 8b** demonstrated the uniform distribution of Ir, Co, and O over a large-scale area without any aggregation phenomena for $\text{Ir}_1\text{-Co}_3\text{O}_4\text{-NS-350}$. HAADF-STEM images revealed less bright atom arrays with some bright atomic columns, confirming the Ir atoms in the spinel Co_3O_4 (**Fig. 8c and d**). First-principles calculations revealed that the hydrogen-bonding interaction between oxygen-containing intermediates and lattice oxygen coordinated to the Ir single atoms effectively reduced the energy barrier for $\ast\text{OOH}$ group formation, thereby accelerating the OER process. Similarly, Qiao and co-workers successfully allocated Ir single atoms into the cationic sites of cobalt spinel oxide via an ion exchange pyrolysis procedure mediated by metal-organic frameworks¹²⁵. The strong interaction between Ir and cobalt oxide support imparts significant corrosion resistance to the catalyst under acidic and oxidative conditions. Huang and his colleagues mixed metal salts with a dispersed Super P carbon substrate, and subsequently achieved the preparation of atomic Ru-doped NiCo alloy ($\text{NiCoRu}_n/\text{SP}$) through low-temperature nucleation (**Fig. 8e and f**)¹³⁸. They found that the excellent HER performance was attributed to the synergistic effect at the Ru-Ni/Co interface,

View Article Online
DOI: 10.1039/D4TA02585G

facilitating electron transfer from atomic Ru to its surrounding Ni/Co.

View Article Online
DOI: 10.1039/D4TA02585G

Another synthesis approach involves the initial preparation of nanoparticles followed by the introduction of single atoms into them. For instance, Zhang et al. conducted the synthesis of double transition metal MXene nanosheets-Mo₂TiC₂T_x with abundant exposed basal planes and outer Mo vacancies using an electrochemical exfoliation method (Mo₂TiC₂T_x-Pt_{SA}, **Fig. 8g**)¹⁰⁶. The created Mo vacancies are used to immobilize single Pt atoms, thereby enhancing the MXene's catalytic activity towards HER. HAADF-STEM images confirm the precise immobilization of Pt atoms at the Mo position on Mo₂TiC₂T_x (**Fig. 8h**). Additionally, EXAFS results demonstrate the presence of Pt in the form of single atoms (**Fig. 8i**). The presence of strong covalent interactions between the positively charged Pt single atoms and MXene contributes to the improvement of catalytic performance and stability.

To sum up, in this section, we classify and discuss the current SA/NPCs based on substrates (i.e., carbon and metal-based carriers) and spatial distribution of nanoparticles and single atoms. These distinct structural characteristics play a pivotal role in enhancing the catalyst's activity and stability. Notably, the carbon-based catalysts with a wrapping configuration exhibit exceptional stability, thus offering significant advantages for potential practical applications. Despite the great promise of SA/NPCs, it should be emphasized that it remains challenging to synthesize SA/NPCs with architected nanostructures. First of all, it is difficult to precisely control the amount of metal precursor introduced. This is a critical factor for the formation of single atoms and nanoparticles, requiring fine-tuned adjustments. For the synthesis of carbon-based SA/NPCs, pyrolysis is commonly adopted, but constructing a structure where nanoparticles are directly anchored to single atoms is nontrivial. In such cases, the formation of metal-oxygen-metal or metal-metal bonds is often necessary to improve

the catalyst's stability. Furthermore, building single-atom and nanoparticle composites with different elemental compositions is more complex than homogeneous systems. Strategies such as coordination and stacking need to be considered in these cases. For the synthesis of metal nanoparticles-based SA/NPCs, there are relatively limited research, and the available synthesis methods are also subject to certain constraints. Overall, the development of SA/NPCs is still in the early stage, and more efforts are required to develop innovative methods to synthesize SA/NPCs with diverse compositions and structures. It is suggested that establishing the process-structure relationship will be helpful in promoting the development of this type of catalysts.

[View Article Online](#)
DOI: 10.1039/D4TA02585G

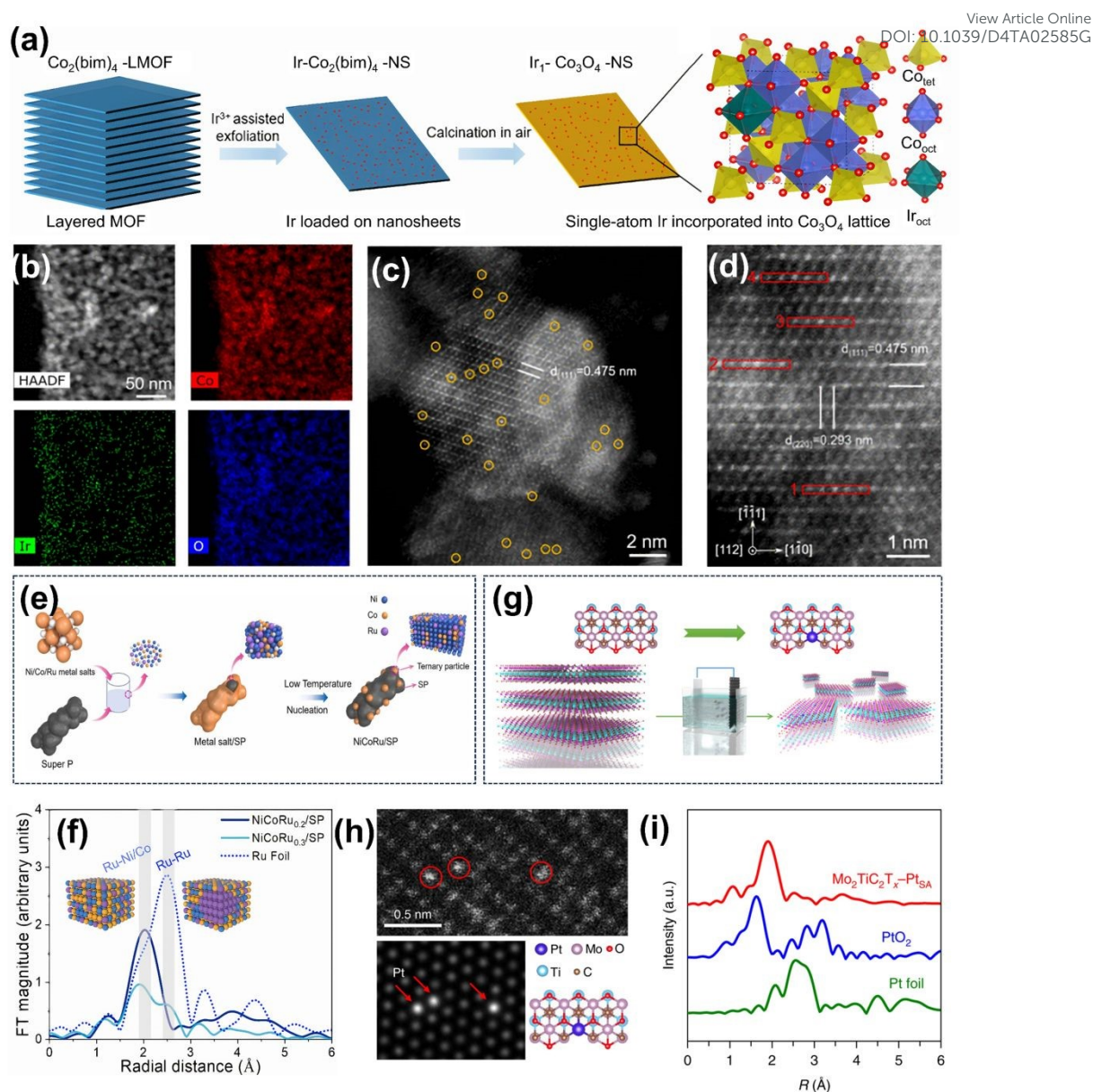


Fig. 8. (a) Schematic route for the synthesis of $\text{Ir}_1\text{-Co}_3\text{O}_4\text{-NS}$. (b) HAADF-STEM image of $\text{Ir}_1\text{-Co}_3\text{O}_4\text{-NS-NS-350}$ and the corresponding EDS elemental mapping images. (c) HAADF-STEM image of $\text{Ir}_1\text{-Co}_3\text{O}_4\text{-NS-NS-350}$, in which the bright spots highlighted by yellow circles are ascribed to Ir single atoms. (d) Atomic-scale HAADF-STEM image of $\text{Ir}_1\text{-Co}_3\text{O}_4\text{-NS-NS-350}$ from the zone axis. Reproduced from Ref. ¹²⁴, Copyright 2023 American Chemical Society. (e) Schematic diagram of synthesis of NiCoRu/SP . (f) FT-EXAFS R-space spectra of $\text{NiCoRu}_{0.2}/\text{SP}$, $\text{NiCoRu}_{0.3}/\text{SP}$ and Ru Foil. Reproduced from Ref. ¹³⁸, Copyright 2023 Elsevier. (g) Schematic diagram of synthesis of $\text{Mo}_2\text{TiC}_2\text{T}_x\text{-Pt}_{\text{SA}}$. (h) Magnified HAADF-STEM image of $\text{Mo}_2\text{TiC}_2\text{T}_x\text{-Pt}_{\text{SA}}$ and its corresponding simulated image. (i) FT-EXAFS spectra of Pt foil, PtO_2 and $\text{Mo}_2\text{TiC}_2\text{T}_x\text{-Pt}_{\text{SA}}$. Reproduced from Ref. ¹⁰⁶, Copyright 2018 Nature.

4. Applications of SA/NPCs

View Article Online
DOI: 10.1039/D4TA02585G

The above discussion on the integrated effects and structural features of SA/NPCs clearly evidence that these catalysts have significant potential in the field of electrochemical energy conversion and storage. In this section, we will primarily delve into the specific applications of SA/NPCs as catalysts for ORR, OER, and HER. Additionally, we will explore their utilization as bifunctional catalysts in rechargeable ZABs and overall water-splitting devices. Furthermore, the latest advancements in the implementation of SA/NPCs as trifunctional catalysts and in emerging catalytic reactions (e.g., carbon dioxide and nitrogen reduction reactions) will also be examined and discussed. **Table S1** summarizes and compares the ORR, OER, and HER performance of some recently reported SA/NPCs.

4.1 Oxygen reduction reaction

ORR is a crucial half-reaction for next-generation renewable energy storage and conversion devices, such as fuel cells¹³⁹ and metal-air batteries^{101, 140, 141}. The thermodynamics and kinetics of ORR play a decisive role in determining the actual efficiency and stability of these devices. Depending on the number of transferred electrons, ORR can be divided into two pathways: a four-electron process toward $\text{H}_2\text{O}/\text{OH}^-$ and a two-electron process toward $\text{H}_2\text{O}_2/\text{HO}_2^-$ in alkaline and acidic medium, respectively^{140, 142, 143}. Compared to the two-electron pathway, which produces harmful peroxides that are not conducive to the stability of the cells, the four-electron pathway is more desired because it yields higher energy output and avoids the formation of harmful intermediate species¹⁴⁴. However, the four-electron pathway of ORR involves complex electron transfer and oxygen-oxygen bond-breaking processes, resulting in sluggish kinetics, therefore requiring the use of electrocatalysts to overcome the reaction energy barrier^{145, 146}. The mechanism for the four-electron reaction process is

shown in **Table 2** (* denotes active sites) ^{147, 148}.

View Article Online
DOI: 10.1039/D4TA02585G

Table 2. Reaction mechanism of four-electron ORR in alkaline and acidic media.

Mechanism	Alkaline medium	Acidic medium
Dissociative	$\begin{aligned} & \text{O}_2 + 2^* \rightarrow 2^*\text{O} \\ & 2^*\text{O} + 2\text{H}_2\text{O} + 2\text{e}^- \rightarrow 2^*\text{OH} + 2\text{OH}^- \\ & 2^*\text{OH} + 2\text{e}^- \rightarrow 2\text{OH}^- + 2^* \end{aligned}$	$\begin{aligned} & \text{O}_2 + 2^* \rightarrow 2^*\text{O} \\ & 2^*\text{O} + 2\text{e}^- + 2\text{H}^+ \rightarrow 2^*\text{OH} \\ & 2^*\text{OH} + 2\text{e}^- + 2\text{H}^+ \rightarrow 2\text{H}_2\text{O} + 2^* \end{aligned}$
Associative	$\begin{aligned} & ^* + \text{O}_2 \rightarrow ^*\text{O}_2 \\ & ^*\text{O}_2 + \text{H}_2\text{O} + \text{e}^- \rightarrow ^*\text{OOH} + \text{OH}^- \\ & ^*\text{OOH} + \text{e}^- \rightarrow ^*\text{O} + \text{OH}^- \\ & ^*\text{O} + \text{H}_2\text{O} + \text{e}^- \rightarrow ^*\text{OH} + \text{OH}^- \\ & ^*\text{OH} + \text{e}^- \rightarrow ^* + \text{OH}^- \end{aligned}$	$\begin{aligned} & \text{O}_2 + ^* \rightarrow ^*\text{O}_2 \\ & ^*\text{O}_2 + \text{H}^+ + \text{e}^- \rightarrow ^*\text{OOH} \\ & ^*\text{OOH} + \text{H}^+ + \text{e}^- \rightarrow ^*\text{O} + \text{H}_2\text{O} \\ & ^*\text{O} + \text{H}^+ + \text{e}^- \rightarrow ^*\text{OH} \\ & ^*\text{OH} + \text{H}^+ + \text{e}^- \rightarrow \text{H}_2\text{O} + ^* \end{aligned}$

There is no doubt that effectively controlling the generation of ORR intermediates is the key to accelerating four-electron ORR, especially regulating the adsorption energy of the intermediates ¹⁴⁹. Therefore, it is necessary to effectively tailor the structure of the catalysts to reduce the energy barrier of the four-electron pathway and achieve rapid conversion rates. Integrating single atoms with nanoparticles represents an effective way to achieve highly efficient ORR catalysts with high stability due to the above-mentioned effects ^{150, 151}. In this regard, Liu et al. successfully achieved co-doping of Fe single atoms/clusters on N-doped carbon catalysts using a porosity-inducing templates method (denoted as Fe/NC, **Fig. 9a**) ¹⁵². Benefiting from the unique structural features, large surface area, and the synergetic effect of Fe single atom and nanocluster, Fe/NC exhibited outstanding ORR activity in both acidic and alkaline media (**Fig. 9b and c**), along with excellent stability during a 20-hour test. Theoretical calculations revealed that the presence of metallic Fe clusters in the catalyst plays a crucial role in electron transfer to the carbon matrix, which imposes a positive effect of downshifting the d-band center and optimizing the binding energy of the ORR intermediates, thus enhancing catalytic kinetics. However, Fe-based catalysts often undergo Fenton reactions (Fe and H₂O₂ reactions), which, unfortunately, result in the degradation of membranes and catalytic electrodes ¹⁵³. To mitigate this issue,

researchers have sought to explore alternative ORR catalysts, such as Co-based catalysts that are less hazardous. For example, Wang et al. utilized a simple method involving the pyrolysis of metal-organic frameworks to obtain both atomically dispersed Co single atoms (Co-SAs) and small Co nanoparticles (Co-SNPs) anchored on nitrogen-doped porous carbon nanocage (Co-SAs/SNPs@NC, **Fig. 9d**)¹⁵⁴. The resulting Co-SAs/SNPs@NC catalyst demonstrated excellent ORR activity in alkaline media, exhibiting a positive half-wave potential ($E_{1/2}$, the potential at the half of limiting current density value for ORR) of 0.898 V (**Fig. 9e**). Moreover, the catalyst showed excellent durability, retaining 96.51% of the initial current after 96-hour test (**Fig. 9f**). The enhanced performance can be attributed to the synergistic effect between Co-SAs and Co-SNPs and the higher degree of carbon graphitization in Co-SAs/SNPs@NC resulting from the introduction of small Co-SNPs. DFT calculations indicated that the strong interaction between Co-SNPs and Co-N₄ molecules significantly increase the valence of active Co atoms in Co-SAs/SNPs@NC, thereby moderating the adsorption free energy of ORR intermediates and promoting the reduction of O₂. In addition to the combination of single atoms of the same metal and nanoparticles mentioned above, the integration of single atoms with metal alloy nanoparticles has also been explored¹⁵⁵⁻¹⁵⁷. Notably, hybrid electrocatalysts that combine PtFe or Pt₃Co alloy nanoparticles have shown significant promise in enhancing the durability of the catalysts for ORR in acidic environments^{158, 159}.

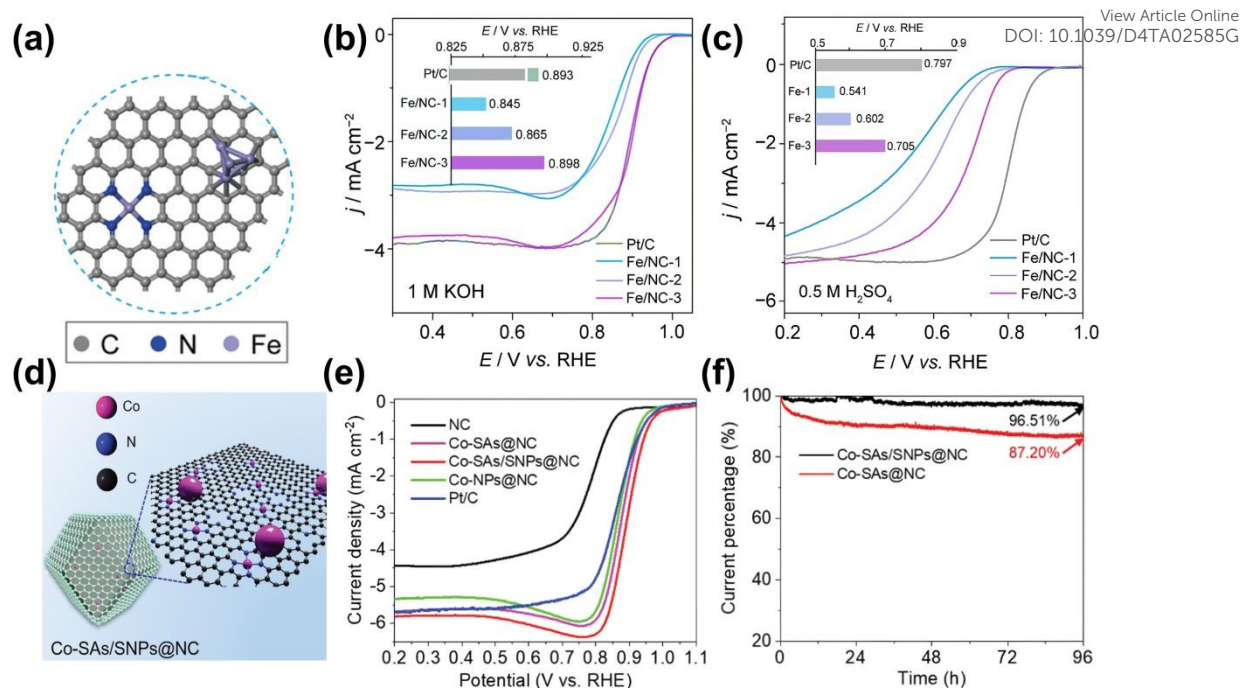


Fig. 9. (a) The model structure of Fe/NC. (b) ORR polarization curves. Inset is the half-wave potentials obtained from the polarization curves. (c) ORR polarization curves of Fe/NC catalysts and Pt/C. Inset shows the half-wave potentials obtained from the polarization curves. Reproduced from Ref. ¹⁵², Copyright 2021 Wiley-VCH. (d) The model structure of Co-SAs/SNPs@NC. (e) ORR polarization curves for Co-SAs/SNPs@NC and references. (f) Chronoamperometric curves of Co-SAs/SNPs@NC and Co-SAs@NC at 0.6 V vs. RHE. Reproduced from Ref. ¹⁵⁴, 2021 Wiley-VCH.

4.2 Oxygen evolution reaction

OER is an important half-reaction in water splitting and rechargeable metal-air batteries ¹⁶⁰⁻¹⁶². As shown in **Table 3**, as the reverse reaction of ORR, OER also involves multi-step single electron transfer reactions in alkaline and acidic electrolytes and shares the same intermediates with ORR ¹⁶³. Multiple electron transfer steps make OER kinetically sluggish and require significant overpotentials to overcome the energy barrier at each step. Generally, the performance of OER is evaluated based on the potential value at 10 mA cm⁻², referred to as $E_{j=10}$. The difference between $E_{j=10}$ and 1.23 V represents the overpotential of the catalysts.

Table 3. Reaction mechanism of OER in alkaline and acidic media.

Alkaline medium	Acidic medium
$* + \text{OH}^- \rightarrow * \text{OH} + \text{e}^-$	$* + \text{H}_2\text{O} \rightarrow * \text{OH} + \text{H}^+ + \text{e}^-$
$* \text{OH} + \text{OH}^- \rightarrow * \text{O} + \text{H}_2\text{O} + \text{e}^-$	$* \text{OH} \rightarrow * \text{O} + \text{H}^+ + \text{e}^-$
$* \text{O} + \text{OH}^- \rightarrow * \text{O O H} + \text{e}^-$	$* \text{O} + \text{H}_2\text{O} \rightarrow * \text{O O H} + \text{H}^+ + \text{e}^-$
$* \text{O O H} + \text{OH}^- \rightarrow * \text{O}_2 + \text{H}_2\text{O} + \text{e}^-$	$* \text{O O H} \rightarrow * \text{O}_2 + \text{H}^+ + \text{e}^-$
$* \text{O}_2 \rightarrow * + \text{O}_2$	$* \text{O}_2 \rightarrow * + \text{O}_2$

Currently, noble metal Ru/Ir-based catalysts are considered the most effective catalysts for OER, but they face problems such as high cost and poor stability¹⁶⁴. Therefore, there is an urgent demand for the development of cost-effective and stable electrocatalysts with high catalytic activity toward OER. One effective approach is to integrate single atoms and nanoparticles in the catalyst design. For example, Liu et al. successfully synthesized efficient electrocatalysts (Ni SAs/Fe-NiOOH) that incorporate dual active sites of NiC₄ single atoms and Fe-NiOOH nanoparticles using the physically adsorbed metal ions method⁹⁰. Ni SAs/Fe-NiOOH exhibited low overpotentials of 269 and 293 mV at current densities of 10 and 50 mA cm⁻², respectively, and demonstrated excellent long-term durability under alkaline conditions (**Fig. 10a and b**). Theoretical calculations confirmed that the excellent OER performance of the catalyst benefits from the tandem catalytic process occurring on the dual active sites of Ni SAs and Fe-NiOOH (**Fig. 10c**).

The integrated form has also been shown to be feasible for the design of OER catalysts in acidic media. For example, Zhu et al. incorporated Ir single atoms into spinel Co₃O₄ (Ir-Co₃O₄) via a mechanochemical method, which displayed a remarkable OER overpotential of 236 mV at the current density of 10 mA cm⁻² and low Tafel slope in an acidic medium (**Fig. 10d and e**)¹⁶⁵. As shown in **Fig. 10f**, Ir-Co₃O₄ also showed long-term stability with a current density of 10 mA cm⁻² for almost 30 h. The operando

X-ray Absorption Spectroscopy (XAS) and DFT results revealed that the existence of high-valence Ir single atoms in Ir- Co_3O_4 is beneficial to charge transferring during the OER process, reducing the energy barrier and thus enhancing the OER activity. Based on the above discussion, it is evident that the binding of single atoms and nanoparticles/clusters has been proven to effectively promote the complex electrocatalytic reaction of OER.

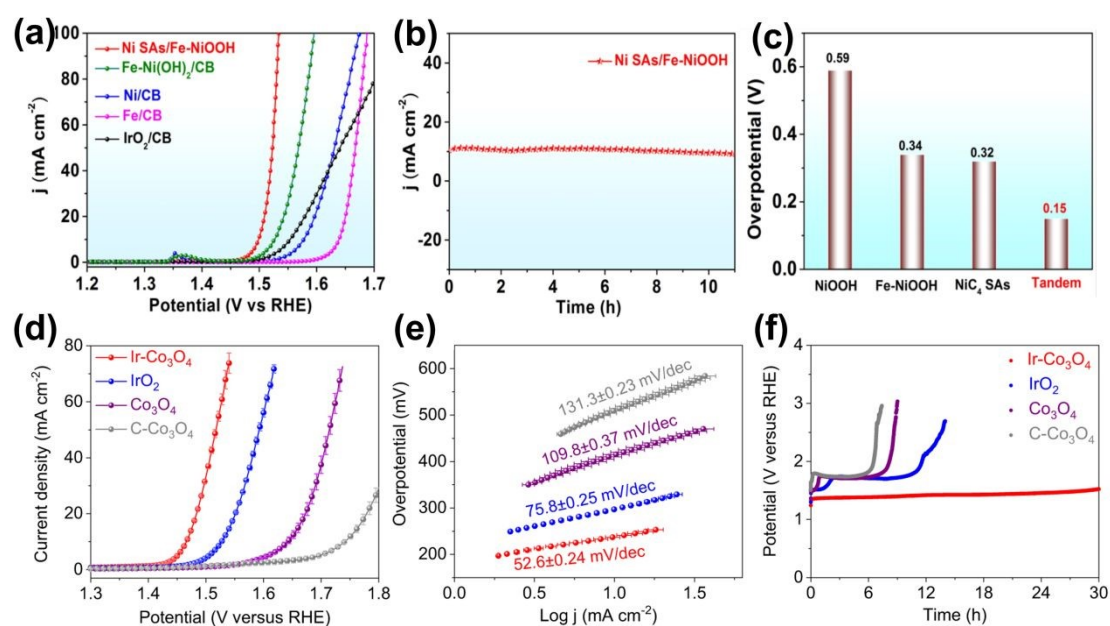


Fig. 10. (a) OER polarization curves of various catalysts in 1.0 M KOH. (b) The stability of Ni SAs/Fe-NiOOH in 1.0 M KOH. (c) The overpotential of different catalysts. (d) OER polarization curves of Ir- Co_3O_4 , IrO_2 , Co_3O_4 and C- Co_3O_4 . Reproduced from Ref. ⁹⁰, Copyright 2021 Elsevier. (e) Tafel plots derived from the polarization curves in (d). (f) Chronopotentiometric measurements of Ir- Co_3O_4 , IrO_2 , Co_3O_4 and C- Co_3O_4 at 10 mA cm⁻², with carbon paper as the catalyst support. Reproduced from Ref. ¹⁶⁵, Copyright 2022 Springer Nature.

4.3 Hydrogen evolution reaction

Hydrogen, with its high specific energy density and renewable nature, holds great promise as an alternative to traditional fossil fuels ¹⁶⁶. Consequently, there has been considerable interest in developing efficient methods for the production and conversion of hydrogen. Among these methods, water electrolysis has emerged as a particularly effective approach for hydrogen production ¹⁶⁷⁻¹⁶⁹. The HER is a half-reaction of water

decomposition, and its specific reaction pathways in different media are shown in **Table 4**.

4¹⁷⁰.

Table 4. Reaction mechanism of HER in alkaline and acidic media.

Mechanism	Alkaline medium	Acidic medium
Volmer step	$* + \text{H}_2\text{O} + \text{e}^- \rightarrow \text{OH}^- + * \text{H}$	$* + \text{H}^+ + \text{e}^- \rightarrow * \text{H}$
Heyrovsky step	$* \text{H} + \text{H}_2\text{O} + \text{e}^- \rightarrow * + \text{OH}^- + \text{H}_2$	$* \text{H} + \text{H}^+ + \text{e}^- \rightarrow * + \text{H}_2$
Tafel step	$2 * \text{H} \rightarrow 2 * + \text{H}_2$	$2 * \text{H} \rightarrow 2 * + \text{H}_2$

HER is both kinetically slow and thermodynamically uphill, requiring electrocatalysts to accelerate the reaction and minimize energy costs. ΔG_{H^*} represents a key indicator in evaluating the activity of HER catalysts. Ideally, high-performance HER electrocatalysts should exhibit a ΔG_{H^*} value approaching zero, facilitating rapid proton/electron transfer and efficient hydrogen desorption¹⁷¹. Although platinum metal has traditionally been recognized as the most effective electrocatalyst for HER due to its favorable adsorption/desorption energy for hydrogen intermediates^{172, 173}, its high cost and stability issues greatly hinder their practical applications. Hence, it is of urgent demand to develop low-cost catalysts with superior electrochemical performances^{174, 175}.

Recent studies have demonstrated that incorporating noble metal atoms into non-precious metal systems can effectively enhance HER activity and reduce catalyst costs. For example, Sultan et al. synthesized a hybrid catalyst (named as: Cu/Rh(SAs) + Cu₂Rh(NPs)/G_N) consisting Cu and Rh elements as bimetallic single atoms and nanoparticles on a N-doped graphene (**Fig. 11a**)¹⁷⁶. This catalyst exhibited excellent HER performance in an acidic medium (**Fig. 11b**) and was expected to be used in acidic electrolyzers for hydrogen production. Moreover, the catalyst showed no significant degradation at current densities of 10, 50 and 100 mA cm⁻² after 500 h of continuous

catalytic electrolysis chronoamperometry testing (**Fig. 11c**). DFT calculations revealed that the combination of Cu and Rh atoms on the graphene matrix not only maximized the rates of hydrogen adsorption on the electrode surface but also optimized the ΔG_{H^*} value close to zero, resulting in a synergistic enhancement of the HER performance. The advantage of combining single atoms and nanoparticles in catalyst design was also evident in their effectiveness for HER in alkaline systems. For instance, Hu et al. designed Ru single atoms and Ru nanoparticles on the Fe/N co-doped carbon (Fe-N-C) substrate, resulting in exceptional HER activity with an incredibly low overpotential of 9 mV to reach current densities of 10 mA cm^{-2} (η_{10}) under alkaline conditions (**Fig. 11d and e**)¹⁷⁷, surpassing that of the state-of-the-art commercial Pt/C catalyst. Remarkably, the catalyst also exhibited a negligible overpotential increase even after 5000 cycles of cyclic voltammetry tests (**Fig. 11f**). Based on DFT calculations, it was found that the single-atom Ru-N₄ moieties significantly improve water dissociation kinetics, while Ru nanoparticles exhibit beneficial effects on hydrogen evolution, leading to a synergistic improvement in alkaline HER performance.

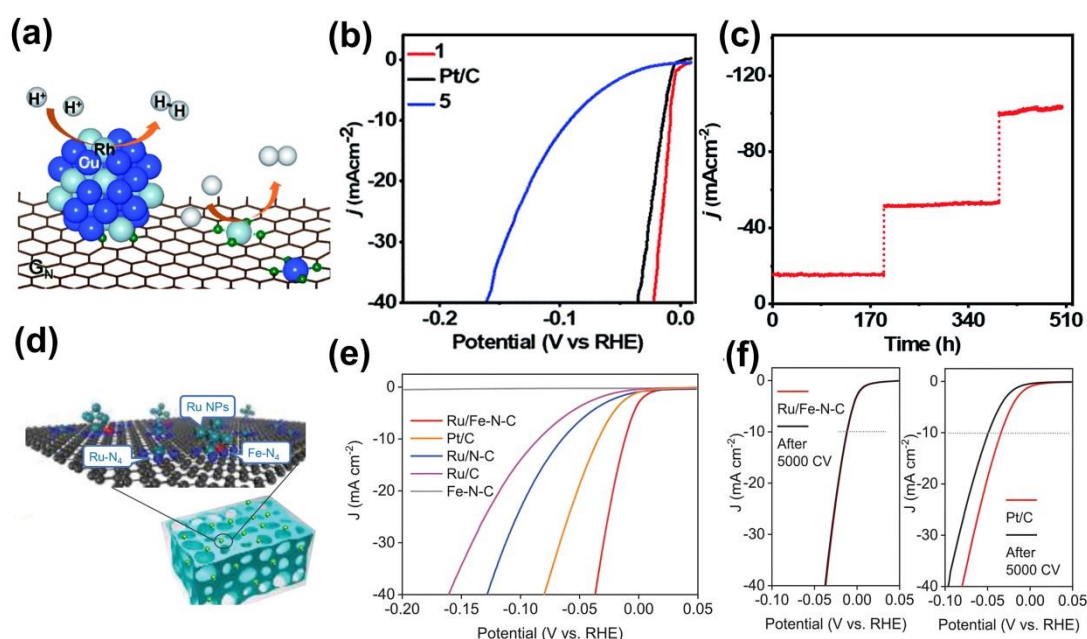


Fig. 11. (a) The model structure of Cu/Rh(SAs) + Cu₂Rh(NPs)/G_N. (b) HER polarization curves of 1-Cu/Rh(SAs) + Cu₂Rh(NPs)/G_N, 5-Rh(SAs) + Rh(NPs)/GN and

commercial Pt/C catalysts. (c) Chronoamperometric response of Cu/Rh(SAs) + Cu₂Rh(NPs)/G_N for 500 hours. (d) The model structure of Ru/Fe-N-C. Reproduced from Ref. ¹⁷⁶, Copyright 2021 Royal Society of Chemistry. (e) HER polarization curves of Ru/Fe-N-C and the control samples. (f) Durability test of Ru/Fe-N-C and Pt/C by recording the polarization curves before and after 5000 cycles. Reproduced from Ref. ¹⁷⁷, Copyright 2020 Wiley-VCH.

4.4 Bi-/tri-functional electrocatalytic applications

4.4.1 Bifunctional ORR/OER for rechargeable zinc-air batteries

Rechargeable ZABs typically consist of zinc anodes, air cathodes, and alkaline aqueous electrolytes (**Fig. 12a**) ¹⁷⁸. This type of device is attracting increasing attention because of its high theoretical capacity (1086 Wh kg⁻¹), high cell voltage (1.65 V), intrinsic safety and environmental friendliness ¹⁷⁹⁻¹⁸². However, the practical application of ZABs is currently severely hindered by high overpotentials at the air cathodes due to the sluggish kinetics of ORR and OER ^{183, 184}. Therefore, the development of catalysts with bifunctional catalytic activity is crucial. The potential gap (ΔE) between $E_{1/2}$ and $E_{j=10}$ serves as the primary parameter for measuring the bifunctional catalytic capability. Lower ΔE values indicate higher energy efficiency and superior bifunctional activity ¹⁸⁵. The development of bifunctional ORR/OER catalysts necessitates the presence of distinct active sites to drive the ORR and OER due to their opposing reaction steps. The integration of single atoms and nanoparticles into a single catalyst system offers the opportunity to introduce diverse active sites or optimize the electronic structure of the active sites, thereby achieving excellent bifunctional ORR/OER activity. To this end, Li et al. employed a dual-phasic carbon nanoarchitecture strategy to synthesize a cobalt-based hybrid catalyst (CNT@CoSA-Co/NCP) ¹⁸⁶. This innovative design incorporates Co single atoms supported on carbon nanotubes and nanosized Co encapsulated in zeolitic-imidazole-framework-derived carbon polyhedron. The presence of the single-atom Co phase greatly enhanced the electroactivity of ORR, while the nanosized Co accelerated the electroactivity of OER.

Consequently, CNT@CoSA-Co/NCP exhibited a substantially smaller ΔE of 0.74 V compared to single-phasic catalysts (CNT@SAC and Co/NCP, **Fig. 12b**). Additionally, when CNT@CoSA-Co/NCP was assembled in a liquid-state ZAB, it achieved a maximum power density of 172 mW cm⁻² (**Fig. 12c**) and exhibited excellent charge-discharge cycling durability with a minimal ΔE decay of 0.09 V after 100 cycles over 33.6 hours of testing. Chandrasekaran et al. provided deeper insights into the intrinsic bifunctional electrocatalytic mechanism of these catalysts through theoretical calculations¹⁸⁷. They used DFT simulations to uncover the strong electronic correlation between Co single atoms and Co nanoparticles within the Co-based catalyst. It was found that the correlation leads to an increased d-electron density near the Fermi level, which effectively optimizes the adsorption and desorption of intermediates in ORR/OER, thereby resulting in an enhanced bifunctional electrocatalytic performance.

Rationally combining bimetallic single-atom sites with nanoparticles is also a promising approach for the development of ORR/OER bifunctional catalysts. Such catalysts offer improved electronic configurations and effective modulation of the binding strength of reaction intermediates¹⁸⁸⁻¹⁹¹. For instance, Zhang et al. synthesized an efficient bifunctional electrocatalyst (SA&NP-FeCo-NTS, **Fig. 12d**)¹⁷⁸. This catalyst features tailored bimetallic atomic FeN₄, CoN₄, along with FeCo alloy nanoparticles, all incorporated within a unique nanotube-assembled-sphere structure. Due to the presence of both atomically dispersed Fe/CoN₄ sites and bimetallic nanoparticles, SA&NP-FeCo-NTS exhibited enhanced catalytic activity, as evidenced by its smallest ΔE value of 0.71 V and 500 discharge and charge cycles for over 250 h (**Fig. 12e**). Xie et al. further combined DFT calculations and demonstrated the significant synergy between bimetallic Fe/Co atoms, FeCo alloy and N-doped carbon frameworks¹⁹². The results demonstrated that the strong synergy has a distinctive

activation effect on the bimetallic Fe/Co atoms, leading to the synchronous modification of the electronic structure and the creation of abundant dual-active Fe/Co-N_x sites to boost reversible oxygen electrocatalysis. Wang et al. successfully synthesized bimetallic NiN₄ and FeN₄ single-atom sites, along with Ni₄ and Fe₄ nanoclusters co-anchored on a highly graphitic carbon support¹⁹³. The hybrid atomic Ni, Fe-DSAs/NCs catalyst exhibited improved activity for ORR/OER, as well as superior stability when compared to their counterparts without nanoclusters and commercial Pt/C. DFT calculations revealed that the Fe₄ clusters induce electron redistribution in the FeN₄ sites and decrease the bonding strength of the Fe-O bond on the central Fe atom. This effect facilitates the desorption of *OH during the ORR process. On the other hand, the Ni₄ clusters increase the total density of states near the Fermi level and enhanced the coupling between the Ni center and oxygen-containing intermediates, thus promoting efficient electron transfer and optimizing the adsorption of *OH on the NiN₄ site during the OER process.

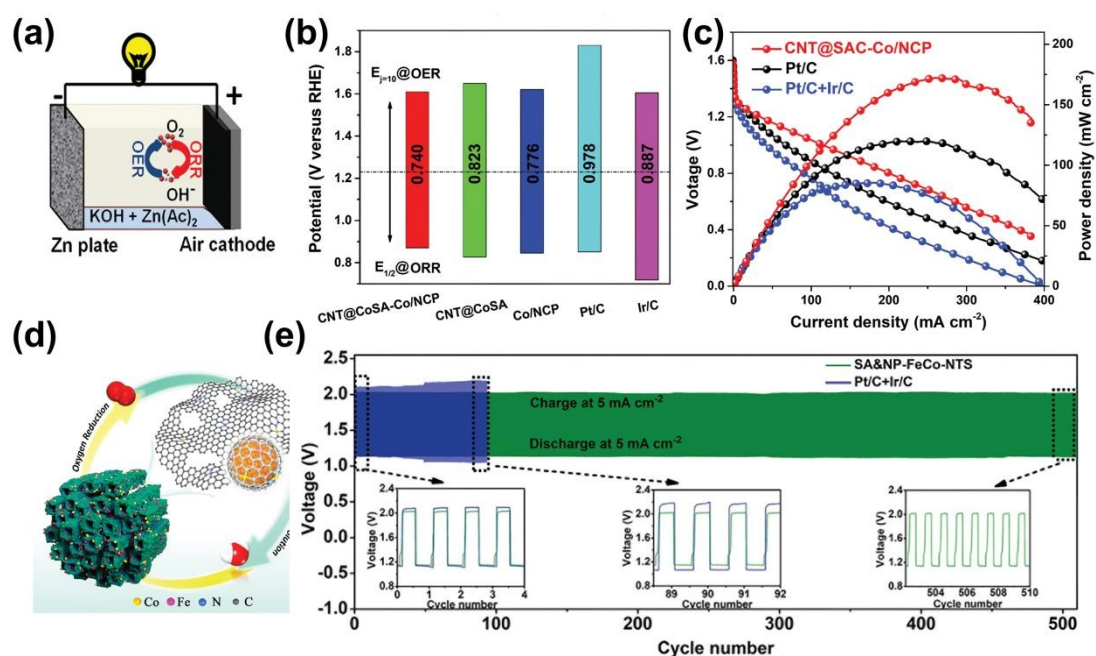


Fig. 12. (a) Schematic of a liquid-state ZAB. Reproduced from Ref.¹⁷⁸, Copyright 2022 Wiley-VCH. (b) Oxygen electrocatalytic performance of CNT@SAC-Co/NCP, CNT@SAC, Co/NCP, Pt/C, and Ir/C. (c) Polarization and power density curves of ZABs using CNT@SAC-Co/NCP, Pt/C, and Pt/C + Ir/C as the oxygen electrocatalysts

(catalyst loading: 0.2 mg cm^{-2}). Reproduced from Ref. ¹⁸⁶, Copyright 2021 Wiley-VCH. View Article Online
DOI: 10.1039/D4TA02585G
 (d) Schematic diagram of the SA&NP-FeCo-NTS. (e) The discharge and charge voltage profiles of ZABs based on SA&NP-FeCo-NTS and Pt/C + Ir/C at 5 mA cm^{-2} and a duration of 30 min per cycle. Inset: the first and last four cycles of galvanostatic charge/discharge cyclic curves based on SA&NP-FeCo-NTS and Pt/C + Ir/C. Reproduced from Ref. ¹⁷⁸, Copyright 2022 Wiley-VCH.

4.4.2 Bifunctional HER/OER for overall water splitting

As mentioned above, electrochemical water splitting is considered a promising technology for industrial-scale hydrogen production toward a sustainable future. This process consists of two crucial processes: the kinetically sluggish HER and OER. Hence, the development of highly efficient catalysts that can simultaneously facilitate both the HER and OER is of utmost importance ^{194, 195}. Recent studies have shown that the synergistic interactions between single atoms and nanoparticles can be instrumental in creating high-performance HER/OER bifunctional electrocatalysts ^{196, 197}. For instance, Luo et al. designed a bifunctional catalyst by incorporating Ni single atoms, Fe single atoms, and NiFe nanoalloys supported on carbon nanotubes ($\text{Ni}_{\text{SA}}\text{Fe}_{\text{SA}}\text{-Ni}_{50}\text{Fe/CNT}$, **Fig. 13a**) ¹⁹⁸. The incorporation of Ni/Fe single atoms in the catalyst enhanced the adsorption/desorption capacity of the intermediate products, while the NiFe nanoalloys generated NiFe (oxy)hydroxides that promoted the OER process. Additionally, the carbon nanotube support served as an effective electrical conductor, facilitating the electron transfer abilities of the catalyst. The synergistic catalysis between single atoms and NiFe nanoparticles, coupled with the robust electron transfer properties, led to the remarkable performance of $\text{Ni}_{\text{SA}}\text{Fe}_{\text{SA}}\text{-Ni}_{50}\text{Fe/CNT}$. It achieved an ultrahigh current density of 382 mA cm^{-2} at a cell voltage of 1.80 V and exhibited the lowest overpotential when compared with other electrocatalytic catalysts for water splitting reported in recent years (**Fig. 13b and c**). Kang and colleagues developed a non-carbon-based HER/OER bifunctional catalyst based on MoS_2 nanosheets ¹⁹⁹. MoS_2 nanosheets are a kind of two-dimensional transition metal dichalcogenide with excellent HER

performance²⁰⁰⁻²⁰². They doped Co atoms into MoS₂ nanosheets and decorated them with Ru nanoparticles (obtaining CoRu-MoS₂ hybrid catalyst, **Fig. 13d**), thus enhancing the bifunctional catalytic activity through this co-doping approach. CoRu-MoS₂ exhibited excellent catalytic activity toward both HER and OER, as characterized by overpotentials of 52 and 308 mV at 10 mA cm⁻² in 1.0 M KOH, respectively (**Fig. 13e and f**). Gibbs free energy (ΔG) calculations confirmed that H₂O dissociation and H₂ production were most favorable on the (002) facet of Ru nanoparticles. The presence of doped Co atoms further catalyzed HER by enhancing the favorability of intermediates. Additionally, the oxidation of Ru nanoparticles resulted in the formation of RuO₂ nanoparticles, which served as active catalytic sites for OER. As a result, the atomic Co-doped MoS₂ and the catalytically active Ru nanoparticles contributed to an optimized electronic structure for efficient water splitting.

4.4.3 Trifunctional HER/OER/ORR

In addition to being used as single or bifunctional catalysts, SA/NPCs even show potential application as trifunctional catalysts. For example, Hong et al. designed a self-supporting trifunctional electrode integrated with Co atoms and clusters, which can be applied to all-solid-state ZABs and self-powered water splitting²⁰³. Li et al. integrated Co single atoms and Co₉S₈ nanoparticles into hollow carbon nanotubes (CoSA + Co₉S₈/HCNT, **Fig. 13g**), which demonstrated excellent trifunctional catalytic activity for HER, OER, and ORR simultaneously⁹⁸. Consequently, CoSA + Co₉S₈/HCNT exhibited remarkable performance in driving liquid-state and all-solid-state ZABs as well as overall water splitting devices (**Fig. 13h and i**). However, due to the complexity of reaction processes and active species, and the fact that theoretical calculations are based on simplified catalyst models, further in-depth analysis of the reaction

mechanism of SA/NPC as trifunctional catalysts remains a future research direction. View Article Online
DOI: 10.1039/D4TA02585G

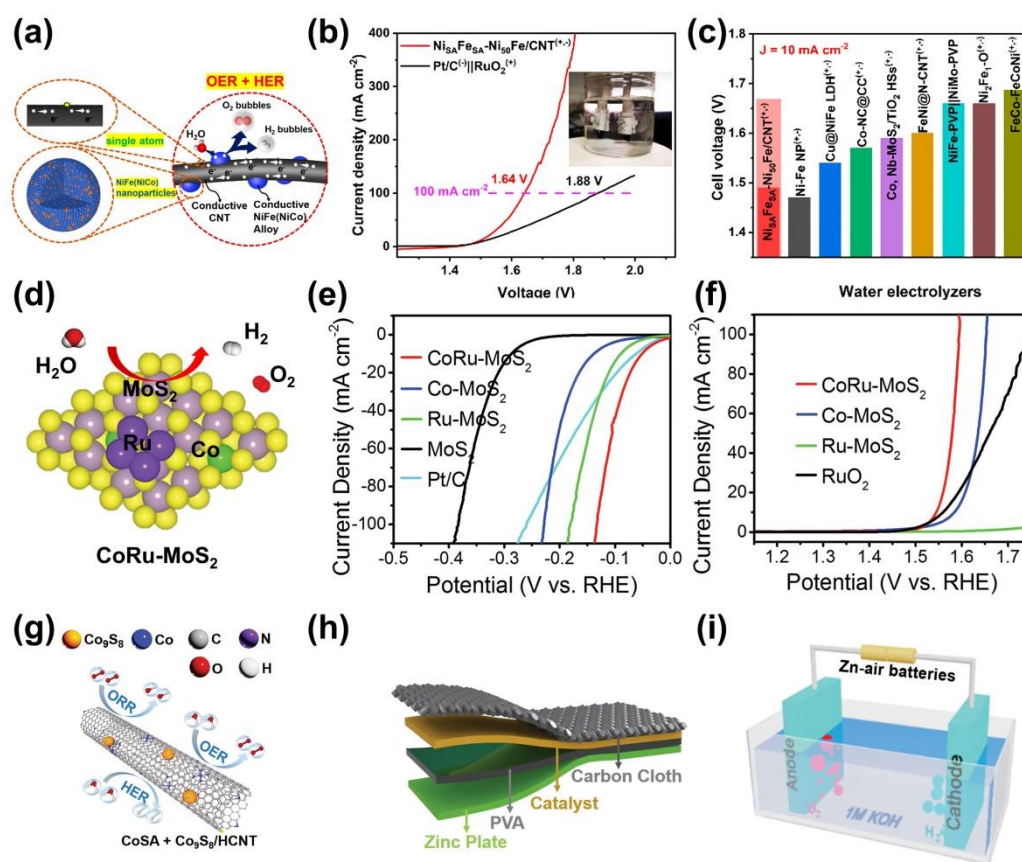


Fig. 13. (a) Schematic diagram of $\text{Ni}_{\text{SA}}\text{Fe}_{\text{SA}}\text{-Ni}_{50}\text{Fe/CNT}$. (b) Comparison of $\text{Ni}_{\text{SA}}\text{Fe}_{\text{SA}}\text{-Ni}_{50}\text{Fe/CN}$ and $\text{Pt/C}||\text{RuO}_2$ for overall water splitting activities at 1 M KOH. Inset is a photograph of electrochemical cell for overall water splitting. (c) Comparison of the cell voltages reaching 10 mA cm^{-2} for different water alkaline electrolyzers. Reproduced from Ref. ¹⁹⁸, Copyright 2022 American Chemical Society. (d) Schematic diagram of CoRu-MoS_2 . (e) HER polarization curves (scan rate: 5 mV s^{-1}) of Co-MoS_2 , Ru-MoS_2 , MoS_2 , and Pt/C in H_2 -saturated 1.0 M KOH. (f) OER polarization curves of Co-MoS_2 , Ru-MoS_2 , MoS_2 , and RuO_2 in O_2 -saturated 1.0 M KOH. Reproduced from Ref. ¹⁹⁹, Copyright 2020 Wiley-VCH. (g) Working mechanism of trifunctional HER/OER/ORR over $\text{CoSA} + \text{Co}_9\text{S}_8/\text{HCNT}$. (h) Schematic diagram of the all-solid-state flexible ZAB. (i) Schematic diagram of self-power water splitting electrolyzer. Reproduced from Ref. ⁹⁸, Copyright 2020 Wiley-VCH.

4.5 Other emerging applications

In addition to the catalytic reactions mentioned above, SA/NPCs also show great potential in the frontier research field of heterogeneous electrocatalysis ⁸⁴. For example, researchers have found that constructing Ni single atoms and Ni nanoparticles (nanoclusters) on carbon substrates can serve as an efficient synergistic catalyst for

electrochemically reducing CO₂ to CO. The existence of Ni nanoparticles (nanoclusters) can effectively accelerate the the proton capture process at N-coordinated single-atom active sites (Ni–N_x), thus promoting the overall CO₂ reduction process^{204, 205}. In addition, Ma et al. found that Mo single atoms and Mo₂C nanoparticles exhibit synergistic catalytic activity for nitrogen reduction reaction (NRR)²⁰⁶. Theoretical calculations revealed that Mo₂C nanoparticles are responsible for the high NRR activity, which is attributed to the Mo single atoms building a large *H coverage environment around Mo₂C to activate the N₂ adsorption and improve both the selectivity and activity of the NRR process. Nie et al. designed Ru-nanoclusters-coupled Mn₃O₄ catalysts decorated with Ru single atoms for an electrochemical N₂ oxidation reaction, which produces nitric products from water and atmospheric N₂²⁰⁷. Experiments and DFT calculations suggest that the synergistic effect between Ru and Mn₃O₄ could effectively activate chemically inert N₂ molecules, reduce the energy barrier of the potential determining step, and further regulate the catalytic kinetics for optimized performance. It is worth noting that, in addition to their wide applications in electrocatalysis, SA/NPCs also hold promise in the fields of thermocatalysis^{208, 209}, photocatalysis^{210, 211} and piezoelectric catalysis²¹².

To sum up, various SA/NPCs have been developed and applied in a wide variety of electrocatalytic reactions, including ORR, OER, and HER. Moreover, integrating single atoms and nanoparticles with different active sites allows the catalysts to achieve bifunctional and even trifunctional catalytic activities, which are essential for electrochemical energy storage devices. However, it should be noted that although endowing different catalytic sites (e.g., ORR and OER) in one catalyst may simplify the electrode design for rechargeable batteries, it may result in compromised catalytic performance of the individual reaction. More specifically, because the active sites for

ORR and OER are different, the co-existence of ORR and OER active sites in one catalyst will reduce the number of active sites for ORR or OER compared to that with only active sites for ORR and OER. Therefore, further research may take the rationale of bi-/tri-functional catalysts into consideration.

5. Concluding remarks and perspectives

In summary, recent advances in the integration of single atoms and nanoparticles (clusters) as highly efficient catalysts for electrochemical energy conversion are reviewed. It has been shown that the individual active species do not just combine to offer more reactive sites but work collectively/synergistically via the electron transfer effect, tandem effect, and parallel effect to greatly enhance the electrocatalytic activity, selectivity, and stability of the catalysts. These integrated catalytic entities, composed of two or more types of active species, provide distinct advantages for numerous reactions involving multiple pathways or steps. As a result, they have been widely reported to be used in various electrocatalytic reactions, such as ORR, OER, HER, which are crucial for fuel cells, metal-air batteries, and overall water splitting devices. Despite substantial progress in this category of catalysts, significant challenges remain, and some perspectives are highlighted as follows:

(1) A vast variety of studies have shown that the catalytic properties strongly depend on the electronic and geometrical structure of the catalysts. The investigation of the interactions between single atoms and nanoparticles and their role in catalytic properties is still nascent. While electron transfer between them has been observed, the existence of direct bonding and additional interactions remains elusive. Therefore, exploring the constituent structures in hybrid catalysts is crucial to guide the analysis of the catalytic mechanism. Some advanced characterization techniques, such as direct detection electron energy loss spectroscopy and temporal analysis of products (TAP),

would be helpful to achieve this goal.

View Article Online
DOI: 10.1039/D4TA02585G

(2) The creation of highly active and stable single-atom and nanoparticle hybrid catalysts necessitates detailed characterization of the composition and structure of the active species. Static condition characterizations can be efficiently performed using HAADF-STEM and EXAFS, but probing the structural changes in dynamic processes poses great challenges. This difficulty arises from the evolution of the active site at high current densities and overpotentials. More efforts are needed to advance atomic-resolution and surface-sensitive characterization techniques for gaining insights into the active center structure and reaction mechanisms. For example, in-situ/operando spectroelectrochemical techniques could be employed to detect the dynamic evolution of active sites.

(3) More accurate theoretical models are highly required to uncover the mechanisms of catalytic reactions. Currently, many studies rely on simplified theoretical models, overlooking crucial factors such as solvation effects, working pH, and applied potential²¹³. To gain a more comprehensive understanding of the evolution of electronic structures and adsorption behaviors in real catalytic processes, more rigorous theoretical models should be developed for in-depth investigation. Combining machine learning techniques with first-principles calculations is a promising approach that can efficiently screen and optimize the positions and coordination environments of atoms within catalysts, resulting in more accurate theoretical models. Based on a large amount of electrocatalytic experimental data and calculation results, machine learning algorithms have the potential to discover the correlation between catalyst structure and performance, and provide valuable guidance for catalyst design. Furthermore, molecular dynamics simulations offer a powerful tool to simulate the impact of solvent environments on catalytic processes, which can provide insights into the dynamic

behavior and stability of catalytic systems in realistic conditions.

View Article Online
DOI: 10.1039/D4TA02585G

It is believed that addressing the above challenges will unleash the full potential of this promising type of catalyst for various applications. Moreover, compared to their individual components, the development of integrated catalysts remains in its infancy, leaving ample room for exploration, e.g., diverse combinations of single atoms with various nanoparticle types (carbides, nitrides, phosphides, alloys, etc.), utilizing bimetallic single atoms, introducing heteroatoms, and other forms to design multifunctional catalysts. Given their unique synergistic properties, it is anticipated that the integration of single atoms with nanoparticle catalysts could play a significant role in meeting the rigorous demands of next-generation energy conversion.

Acknowledgment

The work described in this paper was largely supported by a grant from the Research Grants Council of the Hong Kong Special Administrative Region, China (Project No. 16205822). This work was also financially supported by the Guangdong Basic and Applied Basic Research Foundation (No. 2022B1515120004), and the Shenzhen Science and Technology Plan Project (No. KCXST20221021111406016).

References

1. T. Najam, S. S. A. Shah, S. Ibraheem, X. Cai, E. Hussain, S. Suleman, M. S. Javed and P. Tsiakaras, *Energy Stor. Mater.*, 2022, **45**, 504-540.
2. J. Tong, W. Ma, L. Bo, T. Li, W. Li, Y. Li and Q. Zhang, *J. Power Sources*, 2019, **441**, 227166.
3. S. Maiti, K. Maiti, M. T. Curnan, K. Kim, K.-J. Noh, J. W. Han and S. Maiti, *Energy Environ. Sci.*, 2021, **14**, 3717-3756.
4. H. Li, Y. Guo and Z. Jin, *Carbon Neutrality*, 2023, **2**, 22.
5. T. Wang, X. Cao and L. Jiao, *Carbon Neutrality*, 2022, **1**, 21.
6. S. Park, Y. Shao, J. Liu and Y. Wang, *Energy Environ. Sci.*, 2012, **5**, 9331-9344.
7. J. Suntivich, H. A. Gasteiger, N. Yabuuchi, H. Nakanishi, J. B. Goodenough and Y. Shao-Horn, *Nature Chem.*, 2011, **3**, 546-550.
8. N. Zhang, X. Zhang, L. Tao, P. Jiang, C. Ye, R. Lin, Z. Huang, A. Li, D. Pang and H. Yan, *Angew. Chem. Int. Ed. Engl.*, 2021, **60**, 6170-6176.
9. J. Xue, S. Deng, R. Wang and Y. Li, *Carbon*, 2023, **205**, 422-434.

10. J. Xue, Z. Liu, Y. Fan, R. Wang and Y. Li, *Chem. Eng. J.*, 2023, **476**, 146502. View Article Online
DOI: 10.1039/D4TA02585G
11. J. Xue, Z. Liu and Y. Li, *J. Energy Storage*, 2023, **74**, 109343.
12. A. Morozan, B. Josselme, S. Palacin and A. Morozan, *Energy Environ. Sci.*, 2011, **4**, 1238-1254.
13. T. Wang, A. Chutia, D. J. L. Brett, P. R. Shearing, G. He, G. Chai, I. P. Parkin and T. Wang, *Energy Environ. Sci.*, 2021, **14**, 2639-2669.
14. E. Auer, A. Freund, J. Pietsch and T. Tacke, *Appl Catal A-gen*, 1998, **173**, 259-271.
15. M. A. Hubert, L. A. King and T. F. Jaramillo, *ACS Energy Lett.*, 2021, **7**, 17-23.
16. Z.-B. Wang, P.-J. Zuo, Y.-Y. Chu, Y.-Y. Shao and G.-P. Yin, *Int. J. Hydrog. Energy*, 2009, **34**, 4387-4394.
17. B. Genorio, R. Subbaraman, D. Strmcnik, D. Tripkovic, V. R. Stamenkovic and N. M. Markovic, *Angew. Chem. Int. Ed. Engl.*, 2011, **50**, 5468-5472.
18. Z. Xia, S. Guo and Z. Xia, *Chem. Soc. Rev.*, 2019, **48**, 3265-3278.
19. X. Lin, Y. Hu, K. Hu, X. Lin, G. Xie, X. Liu, K. M. Reddy and H.-J. Qiu, *ACS Mater. Lett.*, 2022, **4**, 978-986.
20. X. Lin, G. Chen, Y. Zhu and H. Huang, *Energy Reviews*, 2024, 100076.
21. X. Lin, Q. Li, Y. Hu, Z. Jin, K. M. Reddy, K. Li, X. Lin, L. Ci and H. J. Qiu, *Small*, 2023, **19**, 2300612.
22. T. Sun, S. Mitchell, J. Li, P. Lyu, X. Wu, J. Pérez-Ramírez and J. Lu, *Adv. Mater.*, 2021, **33**, 2003075.
23. Z. Xu, H. Zhang, H. Zhong, Q. Lu, Y. Wang and D. Su, *Appl. Catal. B*, 2012, **111-112**, 264-270.
24. I. E. Wachs, *J Catal*, 2022, **405**, 462-472.
25. Y. Lykhach, S. M. Kozlov, T. Skála, A. Tovt, V. Stetsovykh, N. Tsud, F. Dvořák, V. Johánek, A. Neitzel, J. Mysliveček, S. Fabris, V. Matolín, K. M. Neyman and J. Libuda, *Nat. Mater.*, 2015, **15**, 284-288.
26. L. Tang, M. Xia, S. Cao, X. Bo, S. Zhang, Y. Zhang, X. Liu, L. Zhang, L. Yu and D. Deng, *Nano Energy*, 2022, **101**, 107562.
27. Y. Zhang, Q. Zhou, J. Zhu, Q. Yan, S. X. Dou and W. Sun, *Adv. Funct. Mater.*, 2017, **27**, 1702317.
28. A. Ali, F. Long and P. K. Shen, *Electrochem. Energy Rev.*, 2022, **5**, 1.
29. F. Su, Z. Tian, C. K. Poh, Z. Wang, S. H. Lim, Z. Liu and J. Lin, *Chem. Mater.*, 2009, **22**, 832-839.
30. C. Tang, A. Sun, Y. Xu, Z. Wu and D. Wang, *J. Power Sources*, 2015, **296**, 18-22.
31. C. Wang, D. van der Vliet, K.-C. Chang, H. You, D. Strmcnik, J. A. Schlueter, N. M. Markovic and V. R. Stamenkovic, *J. Phys. Chem. C*, 2009, **113**, 19365-19368.
32. H. Wang, H.-W. Lee, Y. Deng, Z. Lu, P.-C. Hsu, Y. Liu, D. Lin and Y. Cui, *Nat. Commun.*, 2015, **6**, 7261.
33. B. Roldan Cuenya and F. Behafarid, *Surf. Sci. Rep.*, 2015, **70**, 135-187.
34. H. Song, Y. Li, L. Shang, Z. Tang, T. Zhang and S. Lu, *Nano Energy*, 2020, **72**, 104730.
35. L. Bu, Q. Shao, B. E. J. Guo, J. Yao and X. Huang, *J. Am. Chem. Soc.*, 2017, **139**, 9576-9582.
36. L.-N. Zhang, Z.-L. Lang, Y.-H. Wang, H.-Q. Tan, H.-Y. Zang, Z.-H. Kang, Y.-G. Li and L.-N. Zhang, *Energy Environ. Sci.*, 2019, **12**, 2569-2580.
37. Z. Peng and H. Yang, *Nano Today*, 2009, **4**, 143-164.

38. R. Reske, H. Mistry, F. Behafarid, B. Roldan Cuenya and P. Strasser, *J. Am. Chem. Soc.*, 2014, **136**, 6978-6986. View Article Online
DOI: 10.1039/D4TA02585G
39. W. Rong, H. Zou, W. Zang, S. Xi, S. Wei, B. Long, J. Hu, Y. Ji and L. Duan, *Angew. Chem. Int. Ed. Engl.*, 2021, **60**, 466-472.
40. G. Zhao, F. Yang, Z. Chen, Q. Liu, Y. Ji, Y. Zhang, Z. Niu, J. Mao, X. Bao, P. Hu and Y. Li, *Nat. Commun.*, 2017, **8**, 14039.
41. W.-P. Zhou, S. Axnanda, M. G. White, R. R. Adzic and J. Hrbek, *J. Phys. Chem. C*, 2011, **115**, 16467-16473.
42. J. Wan, D. Liu, H. Xiao, H. Rong, S. Guan, F. Xie, D. Wang, Y. Li and J. Wan, *Commun. Chem.*, 2020, **56**, 4316-4319.
43. X. Li, H. Rong, J. Zhang, D. Wang and Y. Li, *Nano Res.*, 2020, **13**, 1842-1855.
44. J. Yin, J. Jin, H. Liu, B. Huang, M. Lu, J. Li, H. Liu, H. Zhang, Y. Peng, P. Xi and C.-H. Yan, *Adv. Mater.*, 2020, **32**, 2001651.
45. Z. Jiang, T. Wang, J. Pei, H. Shang, D. Zhou, H. Li, J. Dong, Y. Wang, R. Cao, Z. Zhuang, W. Chen, D. Wang, J. Zhang, Y. Li and Z. Jiang, *Energy Environ. Sci.*, 2020, **13**, 2856-2863.
46. X. Bu, X. Liang, K. O. Egbo, Z. Li, Y. Meng, Q. Quan, Y. Y. Li, K. M. Yu, C.-M. L. Wu and J. C. Ho, *Nano Res.*, 2020, **13**, 3130-3136.
47. H. Ou, D. Wang and Y. Li, *Nano Select*, 2021, **2**, 492-511.
48. K. Mori, H. Yamashita and K. Mori, *Phys. Chem. Chem. Phys.*, 2010, **12**, 14420-14432.
49. V. Mazumder, Y. Lee and S. Sun, *Adv. Funct. Mater.*, 2010, **20**, 1224-1231.
50. H. Mistry, A. S. Varela, S. Köhl, P. Strasser and B. R. Cuenya, *Nat. Rev. Mater.*, 2016, **1**, 16009.
51. B. Qiao, A. Wang, X. Yang, L. F. Allard, Z. Jiang, Y. Cui, J. Liu, J. Li and T. Zhang, *Nature Chem.*, 2011, **3**, 634-641.
52. A. Wang, J. Li and T. Zhang, *Nat. Rev. Chem.*, 2018, **2**, 65-81.
53. C. Zhu, S. Fu, Q. Shi, D. Du and Y. Lin, *Angew. Chem. Int. Ed. Engl.*, 2017, **56**, 13944-13960.
54. J. Li, J. Liu and T. Zhang, *Chinese J. Catal.*, 2017, **38**, 1431.
55. F. Li, Y. Bu, G.-F. Han, H.-J. Noh, S.-J. Kim, I. Ahmad, Y. Lu, P. Zhang, H. Y. Jeong and Z. Fu, *Nat. Commun.*, 2019, **10**, 1-7.
56. Y. Chen, Y. Yao, Y. Xia, K. Mao, G. Tang, Q. Wu, L. Yang, X. Wang, X. Sun and Z. Hu, *Nano Res.*, 2020, **13**, 2777-2783.
57. Y.-Q. Su, L. Zhang, Y. Wang, J.-X. Liu, V. Muravev, K. Alexopoulos, I. A. Filot, D. G. Vlachos and E. J. Hensen, *NPJ Comput.*, 2020, **6**, 144.
58. S. Xie, X. Zhang, P. Xu, B. Hatcher, Y. Liu, L. Ma, S. N. Ehrlich, S. Hong and F. Liu, *Catal. Today*, 2022, **402**, 149-160.
59. Z. Xi, K. Shi, X. Xu, P. Jing, B. Liu, R. Gao and J. Zhang, *Adv. Sci.*, 2022, **9**, 2104245.
60. P. Kuang, Y. Wang, B. Zhu, F. Xia, C. W. Tung, J. Wu, H. M. Chen and J. Yu, *Adv. Mater.*, 2021, **33**, 2008599.
61. A. Calderón-Cárdenas, E. A. Paredes-Salazar and H. Varela, *ACS Catal.*, 2020, **10**, 9336-9345.
62. B. Yan, D. Liu, X. Feng, M. Shao and Y. Zhang, *Adv. Funct. Mater.*, 2020, **30**, 2003007.
63. J. N. Tiwari, A. M. Harzandi, M. Ha, S. Sultan, C. W. Myung, H. J. Park, D. Y. Kim, P. Thangavel, A. N. Singh and P. Sharma, *Adv. Energy Mater.*, 2019, **9**, 1970101.
64. J. Ji, Y. Zhang, L. Tang, C. Liu, X. Gao, M. Sun, J. Zheng, M. Ling, C. Liang

- and Z. Lin, *Nano Energy*, 2019, **63**, 103849.
65. X. Yang, Y. Wang, X. Wang, B. Mei, E. Luo, Y. Li, Q. Meng, Z. Jin, Z. Jiang, C. Liu, J. Ge and W. Xing, *Angew. Chem. Int. Ed. Engl.*, 2021, **60**, 26177-26183.
66. P. Li, G. Zhao, P. Cui, N. Cheng, M. Lao, X. Xu, S. X. Dou and W. Sun, *Nano Energy*, 2021, **83**, 105850.
67. C. C. Hou, H. F. Wang, C. X. Li and Q. Xu, *Energy Environ. Sci.*, 2020, **13**, 1658-1693.
68. Q. Hu, G. Li, X. Huang, Z. Wang, H. Yang, Q. Zhang, J. Liu, C. He and Q. Hu, *J. Mater. Chem. A*, 2019, **7**, 19531-19538.
69. X. Ao, W. Zhang, Z. Li, J.-G. Li, L. Soule, X. Huang, W.-H. Chiang, H. M. Chen, C. Wang, M. Liu and X. C. Zeng, *ACS Nano*, 2019, **13**, 11853-11862.
70. C. Lei, Y. Wang, Y. Hou, P. Liu, J. Yang, T. Zhang, X. Zhuang, M. Chen, B. Yang, L. Lei, C. Yuan, M. Qiu, X. Feng and C. Lei, *Energy Environ. Sci.*, 2019, **12**, 149-156.
71. B. Liu, R. Feng, M. Busch, S. Wang, H. Wu, P. Liu, J. Gu, A. Bahadoran, D. Matsumura, T. Tsuji, D. Zhang, F. Song and Q. Liu, *ACS Nano*, 2022, **16**, 14121-14133.
72. Y. Zhang, X. Yu Gao, Z. Wen, C. Cheng Yang and Q. Jiang, *Chem. Eng. J.*, 2022, **446**, 137441.
73. A. Pei, G. Li, L. Zhu, Z. Huang, J. Ye, Y.-C. Chang, S. M. Osman, C.-W. Pao, Q. Gao, B. H. Chen and R. Luque, *Adv. Funct. Mater.*, 2022, **32**, 2208587.
74. X. Zhong, W. Yi, Y. Qu, L. Zhang, H. Bai, Y. Zhu, J. Wan, S. Chen, M. Yang, L. Huang, M. Gu, H. Pan and B. Xu, *Appl. Catal. B*, 2020, **260**, 118188.
75. Z. Li, H. He, H. Cao, S. Sun, W. Diao, D. Gao, P. Lu, S. Zhang, Z. Guo, M. Li, R. Liu, D. Ren, C. Liu, Y. Zhang, Z. Yang, J. Jiang and G. Zhang, *Appl. Catal. B*, 2019, **240**, 112-121.
76. J. Sun, P. Leng, Y. Xie, X. Yu, K. Qu, L. Feng, H. Bao, F. Luo and Z. Yang, *Appl. Catal. B*, 2022, **319**, 121905.
77. T. Zhang, P. Zheng, F. Gu, W. Xu, W. Chen, T. Zhu, Y.-F. Han, G. Xu, Z. Zhong and F. Su, *Appl. Catal. B*, 2023, **323**, 122190.
78. S. H. Yin, J. Yang, Y. Han, G. Li, L. Y. Wan, Y. H. Chen, C. Chen, X. M. Qu, Y. X. Jiang and S. G. Sun, *Angew. Chem. Int. Ed. Engl.*, 2020, **59**, 21976-21979.
79. Y. Liu, J. H. Wu, Y. C. Zhang, X. Jin, J. M. Li, X. K. Xi, Y. Deng, S. H. Jiao, Z. W. Lei, X. Y. Li and R. G. Cao, *ACS Appl. Mater. Interfaces*, 2023, **15**, 14240-14249.
80. F. Mo, Q. Zhou, W. Xue, W. Liu, S. Xu, Z. Hou, J. Wang and Q. Wang, *Adv. Energy Mater.*, 2023, **13**, 2301711.
81. Y. Chen, T. He, Q. Liu, Y. Hu, H. Gu, L. Deng, H. Liu, Y. Liu, Y.-N. Liu, Y. Zhang, S. Chen and X. Ouyang, *Appl. Catal. B*, 2023, **323**, 122163.
82. M. Liu, Y. Ji, Y. Li, P. An, J. Zhang, J. Yan and S. Liu, *Small*, 2021, **17**, 2102448.
83. J. N. Tiwari, A. M. Harzandi, M. Ha, S. Sultan, C. W. Myung, H. J. Park, D. Y. Kim, P. Thangavel, A. N. Singh and P. Sharma, *Adv. Energy Mater.*, 2019, **9**, 1900931.
84. L. Zhang, J. Zhu, X. Li, S. Mu, F. Verpoort, J. Xue, Z. Kou and J. Wang, *Interdiscip. Mater.*, 2022, **1**, 51-87.
85. Z. Liu, L. Zeng, J. Yu, L. Yang, J. Zhang, X. Zhang, F. Han, L. Zhao, X. Li and H. Liu, *Nano Energy*, 2021, **85**, 105940.
86. P. Su, W. Pei, X. Wang, Y. Ma, Q. Jiang, J. Liang, S. Zhou, J. Zhao, J. Liu and G. Q. Lu, *Angew. Chem. Int. Ed. Engl.*, 2021, **60**, 16044-16050.
87. Y. Feng, W. Feng, J. Wan, J. Chen, H. Wang, S. Li, T. Luo, Y. Hu, C. Yuan and

View Article Online
DOI: 10.1039/D4TA02585G

- L. Cao, *Appl. Catal. B*, 2022, **307**, 121193.
88. D. Cao, Z. Zhang, Y. Cui, R. Zhang, L. Zhang, J. Zeng and D. Cheng, *Angew. Chem. Int. Ed. Engl.*, 2023, **62**, e202214259.
89. S. K. Singh, K. Takeyasu and J. Nakamura, *Adv. Mater.*, 2019, **31**, 1804297.
90. H. Liu, X. Xu, H. Xu, S. Wang, Z. Niu, Q. Jia, L. Yang, R. Cao, L. Zheng and D. Cao, *Appl. Catal. B*, 2021, **297**, 120451.
91. J. Zhang, Y. Gu, Y. Lu, C. Zhu, G. Liu, C. Wang, D. Sun, Y. Tang and H. Sun, *Appl. Catal. B*, 2023, **325**, 122316.
92. S. H. Ahn and A. Manthiram, *Small*, 2020, **16**, 2002511.
93. S. C. Ding, L. He, L. Z. Fang, Y. Z. Zhu, T. Li, Z. Y. Lyu, D. Du, Y. H. Lin and J. C. Li, *Adv. Energy Mater.*, 2022, **12**, 2202984.
94. M. W. Louie and A. T. Bell, *J. Am. Chem. Soc.*, 2013, **135**, 12329-12337.
95. B. B. Xu, X. B. Fu, X. M. You, E. Zhao, F. F. Li, Z. P. Chen, Y. X. Li, X. L. Wang and Y. F. Yao, *ACS Catal.*, 2022, **12**, 6958-6967.
96. Y. Q. Sun, J. Q. Luo, M. X. Zhang, J. Li, J. K. Yu, S. Y. Lu, W. Y. Song, Y. C. Wei, Z. X. Li and J. Liu, *ACS Appl. Mater. Interfaces*, 2023, **18**, 10696-10708.
97. J. Liu, C. Wang, H. Sun, H. Wang, F. Rong, L. He, Y. Lou, S. Zhang, Z. Zhang and M. Du, *Appl. Catal. B*, 2020, **279**, 119407.
98. Y. Li, R. Cao, L. Li, X. Tang, T. Chu, B. Huang, K. Yuan and Y. Chen, *Small*, 2020, **16**, 1906735.
99. W. Ye, S. M. Chen, Y. Lin, L. Yang, S. J. Chen, X. S. Zheng, Z. M. Qi, C. M. Wang, R. Long, M. Chen, J. F. Zhu, P. Gao, L. Song, J. Jiang and Y. J. Xiong, *Chem*, 2019, **5**, 2865-2878.
100. D. X. Liu, B. Wang, H. G. Li, S. F. Huang, M. M. Liu, J. Wang, Q. J. Wang, J. J. Zhang and Y. F. Zhao, *Nano Energy*, 2019, **58**, 277-283.
101. F. Yang and W. L. Xu, *J. Mater. Chem. A*, 2022, **10**, 5673-5698.
102. Q. Qin, T. Wang, Z. Li, G. Zhang, H. Jang, L. Hou, Y. Wang, M. G. Kim, S. Liu and X. Liu, *J. Energy Chem.*, 2024, **88**, 94-102.
103. Y. Qin, B. Cao, X.-Y. Zhou, Z. Xiao, H. Zhou, Z. Zhao, Y. Weng, J. Lv, Y. Liu, Y.-B. He, F. Kang, K. Li and T.-Y. Zhang, *Nano Energy*, 2023, **115**, 108727.
104. Y. Zhu, P. Tian, H. Jiang, J. Mu, L. Meng, X. Su, Y. Wang, Y. Lin, Y. Zhu and L. Song, *CCS Chemistry*, 2021, **3**, 2539-2547.
105. Y. Zhao, P. V. Kumar, X. Tan, X. Lu, X. Zhu, J. Jiang, J. Pan, S. Xi, H. Y. Yang and Z. Ma, *Nat. Commun.*, 2022, **13**, 2430.
106. J. Zhang, Y. Zhao, X. Guo, C. Chen, C.-L. Dong, R.-S. Liu, C.-P. Han, Y. Li, Y. Gogotsi and G. Wang, *Nat. Catal.*, 2018, **1**, 985-992.
107. X. Guo, S. Liu and S. Huang, *Int. J. Hydrog. Energy*, 2018, **43**, 4880-4892.
108. L. L. Cao, Q. Q. Luo, J. J. Chen, L. Wang, Y. Lin, H. J. Wang, X. K. Liu, X. Y. Shen, W. Zhang, W. Liu, Z. M. Qi, Z. Jiang, J. L. Yang and T. Yao, *Nat. Commun.*, 2019, **10**, 4849.
109. X. Y. Li, P. Cui, W. H. Zhong, J. Li, X. J. Wang, Z. W. Wang and J. Jiang, *Commun. Chem.*, 2016, **52**, 13233-13236.
110. H. L. Fei, J. C. Dong, Y. X. Feng, C. S. Allen, C. Z. Wan, B. Voloskiy, M. F. Li, Z. P. Zhao, Y. L. Wang, H. T. Sun, P. F. An, W. X. Chen, Z. Y. Guo, C. Lee, D. L. Chen, I. Shakir, M. J. Liu, T. D. Hu, Y. D. Li, A. I. Kirkland, X. F. Duan and Y. Huang, *Nat. Catal.*, 2018, **1**, 63-72.
111. G. P. Gao, S. Bottle and A. J. Du, *Catal. Sci. Technol.*, 2018, **8**, 996-1001.
112. J. Yang, W. Li, D. Wang and Y. Li, *Adv. Mater.*, 2020, **32**, 2003300.
113. L. Kuai, Z. Chen, S. Liu, E. Kan, N. Yu, Y. Ren, C. Fang, X. Li, Y. Li and B. Geng, *Nat. Commun.*, 2020, **11**, 48.

114. X. Wan, Q. Liu, J. Liu, S. Liu, X. Liu, L. Zheng, J. Shang, R. Yu and J. Shui, *Nat. Commun.*, 2022, **13**, 2963. View Article Online
DOI: 10.1039/D4TA02585G
115. L. Zeng, Z. Zhao, Q. Huang, C. Zhou, W. Chen, K. Wang, M. Li, F. Lin, H. Luo, Y. Gu, L. Li, S. Zhang, F. Lv, G. Lu, M. Luo and S. Guo, *J. Am. Chem. Soc.*, 2023, **145**, 21432-21441.
116. P. Cai, Y. Hong, S. Ci and Z. Wen, *Nanoscale*, 2016, **8**, 20048-20055.
117. J. Deng, P. Ren, D. Deng and X. Bao, *Angew. Chem. Int. Ed. Engl.*, 2015, **54**, 2100-2104.
118. X. Cui, P. Ren, D. Deng, J. Deng and X. Bao, *Energy Environ. Sci.*, 2016, **9**, 123-129.
119. S. Li, W. Chen, H. Pan, Y. Cao, Z. Jiang, X. Tian, X. Hao, T. Maiyalagan and Z.-J. Jiang, *ACS Sustain. Chem. Eng.*, 2019, **7**, 8530-8541.
120. L. Chong, J. Wen, J. Kubal, F. G. Sen, J. Zou, J. Greeley, M. Chan, H. Barkholtz, W. Ding and D.-J. Liu, *Science*, 2018, **362**, 1276-1281.
121. Q. Zhang, P. Kumar, X. Zhu, R. Daiyan, N. M. Bedford, K.-H. Wu, Z. Han, T. Zhang, R. Amal and X. Lu, *Adv. Energy Mater.*, 2021, **11**, 2100303.
122. S. N. Zhao, J. K. Li, R. Wang, J. Cai and S. Q. Zang, *Adv. Mater.*, 2022, **34**, 2107291.
123. S. Wang, Z. Lin, M. Li, Z. Yu, M. Zhang, M. Gong, Y. Tang and X. Qiu, *J. Mater. Chem. A*, 2022, **10**, 6086-6095.
124. Y. Liu, Y. W. Chen, X. L. Mu, Z. Y. Wu, X. Jin, J. M. Li, Y. Z. Xu, L. Yang, X. K. Xi, H. Jang, Z. W. Lei, Q. H. Liu, S. H. Jiao, P. F. Yan, X. Y. Li and R. G. Cao, *ACS Catal.*, 2023, **13**, 3757-3767.
125. J. Q. Shan, C. Ye, S. M. Chen, T. L. Sun, Y. Jiao, L. M. Liu, C. Z. Zhu, L. Song, Y. Han, M. Jaroniec, Y. H. Zhu, Y. Zheng and S. Z. Qiao, *J. Am. Chem. Soc.*, 2021, **143**, 5201-5211.
126. Z. Zhang, J. Liu, J. Wang, Q. Wang, Y. Wang, K. Wang, Z. Wang, M. Gu, Z. Tang and J. Lim, *Nat. Commun.*, 2021, **12**, 5235.
127. B. Jiang, X. Ma, M. Liu, Q. Li, X. Xiao, J. Liu, X. Xu, Y. Yin, P. Qiao and L. Zhang, *J. Mater. Chem. A*, 2023, **11**, 16889-16899.
128. R. J. Gao, J. Wang, Z. F. Huang, R. R. Zhang, W. Wang, L. Pan, J. F. Zhang, W. K. Zhu, X. W. Zhang, C. X. Shi, J. Lim and J. J. Zou, *Nat. Energy*, 2021, **6**, 614-623.
129. Y. Hu, J. O. Jensen, W. Zhang, L. N. Cleemann, W. Xing, N. J. Bjerrum and Q. Li, *Angew. Chem. Int. Ed. Engl.*, 2014, **53**, 3675-3679.
130. Z. R. Chen, R. L. Liu, S. H. Liu, J. L. Huang, L. Y. Chen, R. Nadimicherla, D. C. Wu and R. W. Fu, *Commun. Chem.*, 2020, **56**, 12921-12924.
131. Q. Wang, Z. Zhang, C. Cai, M. Wang, Z. L. Zhao, M. Li, X. Huang, S. Han, H. Zhou and Z. Feng, *J. Am. Chem. Soc.*, 2021, **143**, 13605-13615.
132. N. Yang, S. Tian, Y. Feng, Z. Hu, H. Liu, X. Tian, L. Xu, C. Hu and J. Yang, *Small*, 2023, **19**, 2207253.
133. J. Ge, D. He, W. Chen, H. Ju, H. Zhang, T. Chao, X. Wang, R. You, Y. Lin and Y. Wang, *J. Am. Chem. Soc.*, 2016, **138**, 13850-13853.
134. L. Zhou, J. M. P. Martirez, J. Finzel, C. Zhang, D. F. Swearer, S. Tian, H. Robotjazi, M. Lou, L. Dong and L. Henderson, *Nat. Energy*, 2020, **5**, 61-70.
135. K. L. Zhou, Z. Wang, C. B. Han, X. Ke, C. Wang, Y. Jin, Q. Zhang, J. Liu, H. Wang and H. Yan, *Nat. Commun.*, 2021, **12**, 3783.
136. Y. Ren, X. Liu, Z. Zhang, X. Shen and Y. Ren, *Phys. Chem. Chem. Phys.*, 2021, **23**, 15564-15573.
137. X. Cao, Q. Fu, Y. Luo and X. Cao, *Phys. Chem. Chem. Phys.*, 2014, **16**, 8367-

- 8375.
138. L. Li, H. Qiu, Y. Zhu, G. Chen, S. She, X. Guo, H. Li, T. Liu, Z. Lin and H. Zhou, *Appl. Catal. B*, 2023, **331**, 122710.
 139. M. Kannan, *Biosens. Bioelectron.*, 2016, **77**, 1208-1220.
 140. L. Dai, Y. Xue, L. Qu, H.-J. Choi and J.-B. Baek, *Chem. Rev.*, 2015, **115**, 4823-4892.
 141. R. Cao, J. S. Lee, M. Liu and J. Cho, *Adv. Energy Mater.*, 2012, **2**, 816-829.
 142. H. Jin, C. Guo, X. Liu, J. Liu, A. Vasileff, Y. Jiao, Y. Zheng and S.-Z. Qiao, *Chem. Rev.*, 2018, **118**, 6337-6408.
 143. Y. Zheng, Y. Jiao, M. Jaroniec, Y. Jin and S. Z. Qiao, *Small*, 2012, **8**, 3550-3566.
 144. A. A. Razzaq, X. Yuan, Y. Chen, J. Hu, Q. Mu, Y. Ma, X. Zhao, L. Miao, J.-H. Ahn and Y. Peng, *J. Mater. Chem. A*, 2020, **8**, 1298-1306.
 145. Y. Liu, T. G. Kelly, J. G. Chen and W. E. Mustain, *ACS Catal.*, 2013, **3**, 1184-1194.
 146. M. Liu, Z. Zhao, X. Duan and Y. Huang, *Adv. Mater.*, 2019, **31**, 1802234.
 147. J. K. Nørskov, J. Rossmeisl, A. Logadottir, L. Lindqvist, J. R. Kitchin, T. Bligaard and H. Jónsson, *J. Phys. Chem. B*, 2004, **108**, 17886-17892.
 148. Z. W. Seh, J. Kibsgaard, C. F. Dickens, I. Chorkendorff, J. K. Nørskov and T. F. Jaramillo, *Science*, 2017, **355**, eaad4998.
 149. C. A. Etogo, H. Huang, H. Hong, G. Liu and L. Zhang, *Energy Stor. Mater.*, 2020, **24**, 167-176.
 150. W.-J. Jiang, L. Gu, L. Li, Y. Zhang, X. Zhang, L.-J. Zhang, J.-Q. Wang, J.-S. Hu, Z. Wei and L.-J. Wan, *J. Am. Chem. Soc.*, 2016, **138**, 3570-3578.
 151. Y. He, H. Guo, S. Hwang, X. Yang, Z. He, J. Braaten, S. Karakalos, W. Shan, M. Wang, H. Zhou, Z. Feng, K. L. More, G. Wang, D. Su, D. A. Cullen, L. Fei, S. Litster and G. Wu, *Adv. Mater.*, 2020, **32**, 2003577.
 152. M. Liu, J. Lee, T. C. Yang, F. Zheng, J. Zhao, C. M. Yang and L. Y. S. Lee, *Small Methods*, 2021, **5**, 2001165.
 153. D. Banham, T. Kishimoto, Y. Zhou, T. Sato, K. Bai, J.-i. Ozaki, Y. Imashiro and S. Ye, *Sci. Adv.*, 2018, **4**, eaar7180.
 154. Z. Wang, C. Zhu, H. Tan, J. Liu, L. Xu, Y. Zhang, Y. Liu, X. Zou, Z. Liu and X. Lu, *Adv. Funct. Mater.*, 2021, **31**, 2104735.
 155. Z. Xu, G. Chen, F. Yang, J. Jang, G. Liu, F. Xiao, Y. Sun, X. Qiu, W. Chen and D. Su, *Electrochim. Acta*, 2023, **458**, 142549.
 156. X. Ao, W. Zhang, B. Zhao, Y. Ding, G. Nam, L. Soule, A. Abdelhafiz, C. Wang and M. Liu, *Energy Environ. Sci.*, 2020, **13**, 3032-3040.
 157. L. Liang, H. Jin, H. Zhou, B. Liu, C. Hu, D. Chen, Z. Wang, Z. Hu, Y. Zhao and H.-W. Li, *Nano Energy*, 2021, **88**, 106221.
 158. X. Li, Y. He, S. Cheng, B. Li, Y. Zeng, Z. Xie, Q. Meng, L. Ma, K. Kisslinger and X. Tong, *Adv. Mater.*, 2021, **33**, 2106371.
 159. F. Xiao, Q. Wang, G.-L. Xu, X. Qin, I. Hwang, C.-J. Sun, M. Liu, W. Hua, H.-w. Wu and S. Zhu, *Nat. Catal.*, 2022, **5**, 503-512.
 160. D. Yang, L. Zhang, X. Yan and X. Yao, *Small Methods*, 2017, **1**, 1700209.
 161. F. Lu, M. Zhou, Y. Zhou and X. Zeng, *Small*, 2017, **13**, 1701931.
 162. C. Zhu, Q. Shi, S. Feng, D. Du and Y. Lin, *ACS Energy Lett.*, 2018, **3**, 1713-1721.
 163. M. Bajdich, M. García-Mota, A. Vojvodic, J. K. Nørskov and A. T. Bell, *J. Am. Chem. Soc.*, 2013, **135**, 13521-13530.
 164. R. Kötz, H. Lewerenz and S. Stucki, *J. Electrochem. Soc.*, 1983, **130**, 825.

165. Y. Zhu, J. Wang, T. Koketsu, M. Kroschel, J.-M. Chen, S.-Y. Hsu, G. Henkelman, Z. Hu, P. Strasser and J. Ma, *Nat. Commun.*, 2022, **13**, 7754. View Article Online
DOI: 10.1039/D4TA02585G
166. T. Wang, H. Xie, M. Chen, A. D'Aloia, J. Cho, G. Wu and Q. Li, *Nano Energy*, 2017, **42**, 69-89.
167. G. Zhao, K. Rui, S. X. Dou and W. Sun, *Adv. Funct. Mater.*, 2018, **28**, 1803291.
168. Y. Shi and B. Zhang, *Chem. Soc. Rev.*, 2016, **45**, 1529-1541.
169. C. G. Morales-Guio, L.-A. Stern and X. Hu, *Chem. Soc. Rev.*, 2014, **43**, 6555-6569.
170. A. Lasia, *Int. J. Hydrog. Energy*, 2019, **44**, 19484-19518.
171. Y.-Y. Ma, C.-X. Wu, X.-J. Feng, H.-Q. Tan, L.-K. Yan, Y. Liu, Z.-H. Kang, E.-B. Wang and Y.-G. Li, *Energy Environ. Sci.*, 2017, **10**, 788-798.
172. D. Liu, X. Li, S. Chen, H. Yan, C. Wang, C. Wu, Y. A. Haleem, S. Duan, J. Lu and B. Ge, *Nat. Energy*, 2019, **4**, 512-518.
173. J. N. Tiwari, S. Sultan, C. W. Myung, T. Yoon, N. Li, M. Ha, A. M. Harzandi, H. J. Park, D. Y. Kim and S. S. Chandrasekaran, *Nat. Energy*, 2018, **3**, 773-782.
174. N. Cheng, S. Stambula, D. Wang, M. N. Banis, J. Liu, A. Riese, B. Xiao, R. Li, T.-K. Sham and L.-M. Liu, *Nat. Commun.*, 2016, **7**, 13638.
175. A. Kumar, V. Q. Bui, J. Lee, L. Wang, A. R. Jadhav, X. Liu, X. Shao, Y. Liu, J. Yu and Y. Hwang, *Nat. Commun.*, 2021, **12**, 6766.
176. S. Sultan, M. H. Diorizky, M. Ha, J. N. Tiwari, H. Choi, N. K. Dang, P. Thangavel, J. H. Lee, H. Y. Jeong and H. S. Shin, *J. Mater. Chem. A*, 2021, **9**, 10326-10334.
177. C. Hu, E. Song, M. Wang, W. Chen, F. Huang, Z. Feng, J. Liu and J. Wang, *Adv. Sci.*, 2021, **8**, 2001881.
178. Q. Zhang, P. Liu, X. Fu, Y. Yuan, L. Wang, R. Gao, L. Zheng, L. Yang and Z. Bai, *Adv. Funct. Mater.*, 2022, **32**, 2112805.
179. X. Liu, G. Zhang, L. Wang and H. Fu, *Small*, 2021, **17**, 2006766.
180. S. S. Shinde, J. Y. Jung, N. K. Wagh, C. H. Lee, D.-H. Kim, S.-H. Kim, S. U. Lee and J.-H. Lee, *Nat Energy*, 2021, **6**, 592-604.
181. Z. Li, L. Leng, S. Ji, M. Zhang, H. Liu, J. Gao, J. Zhang, J. H. Horton, Q. Xu and J. Zhu, *J. Energy Chem.*, 2022, **73**, 469-477.
182. C. X. Zhao, L. Yu, J. N. Liu, J. Wang, N. Yao, X. Y. Li, X. Chen, B. Q. Li and Q. Zhang, *Angew. Chem. Int. Ed. Engl.*, 2022, **61**, e202208042.
183. Z. Zhao, M. Li, L. Zhang, L. Dai and Z. Xia, *Adv. Mater.*, 2015, **27**, 6834-6840.
184. X. Zhang, X. Cheng and Q. Zhang, *J. Energy Chem.*, 2016, **25**, 967-984.
185. P. Zhang, K. Chen, J. Li, M. Wang, M. Li, Y. Liu and Y. Pan, *Adv. Mater.*, 2023, **35**, 2303243.
186. J. C. Li, Y. Meng, L. Zhang, G. Li, Z. Shi, P. X. Hou, C. Liu, H. M. Cheng and M. Shao, *Adv. Funct. Mater.*, 2021, **31**, 2103360.
187. S. Chandrasekaran, R. Hu, L. Yao, L. Sui, Y. Liu, A. Abdelkader, Y. Li, X. Ren and L. Deng, *Nanomicro Lett*, 2023, **15**, 48.
188. T. Gu, D. Zhang, Y. Yang, C. Peng, D. Xue, C. Zhi, M. Zhu and J. Liu, *Advanced Functional Materials*, 2023, **33**, 2212299.
189. Z. Wang, X. Jin, C. Zhu, Y. Liu, H. Tan, R. Ku, Y. Zhang, L. Zhou, Z. Liu and S. J. Hwang, *Adv. Mater.*, 2021, **33**, 2104718.
190. Z. Zeng, L. Y. Gan, H. Bin Yang, X. Su, J. Gao, W. Liu, H. Matsumoto, J. Gong, J. Zhang and W. Cai, *Nat. Commun.*, 2021, **12**, 4088.
191. Y. Chen, R. Gao, S. Ji, H. Li, K. Tang, P. Jiang, H. Hu, Z. Zhang, H. Hao and Q. Qu, *Angew. Chem. Int. Ed. Engl.*, 2021, **60**, 3212-3221.
192. D. Xie, D. Yu, Y. Hao, S. Han, G. Li, X. Wu, F. Hu, L. Li, H. Y. Chen and Y.

- F. Liao, *Small*, 2021, **17**, 2007239.
193. Z. Wang, X. Jin, R. Xu, Z. Yang, S. Ma, T. Yan, C. Zhu, J. Fang, Y. Liu, S.-J. Hwang, Z. Pan and H. J. Fan, *ACS Nano*, 2023, **17**, 8622-8633.
 194. P. Wang, J. Zhu, Z. Pu, R. Qin, C. Zhang, D. Chen, Q. Liu, D. Wu, W. Li and S. Liu, *Appl. Catal. B*, 2021, **296**, 120334.
 195. D. Guo, Q. Pan, T. Vietor, W. Lu and Y. Gao, *J. Energy Chem.*, 2023, **87**, 518-539.
 196. F. Luo, H. Hu, X. Zhao, Z. Yang, Q. Zhang, J. Xu, T. Kaneko, Y. Yoshida, C. Zhu and W. Cai, *Nano Letters*, 2020, **20**, 2120-2128.
 197. K. Shah, R. Dai, M. Mateen, Z. Hassan, Z. Zhuang, C. Liu, M. Israr, W.-C. Cheong, B. Hu, R. Tu, C. Zhang, X. Chen, Q. Peng, C. Chen and Y. Li, *Angew. Chem. Int. Ed. Engl.*, 2022, **61**, e202114951.
 198. W. Luo, Y. Wang, L. Luo, S. Gong, M. Wei, Y. Li, X. Gan, Y. Zhao, Z. Zhu and Z. Li, *ACS Catal.*, 2022, **12**, 1167-1179.
 199. I. S. Kwon, T. T. Debela, I. H. Kwak, Y. C. Park, J. Seo, J. Y. Shim, S. J. Yoo, J. G. Kim, J. Park and H. S. Kang, *Small*, 2020, **16**, 2000081.
 200. X. Hu, R. Wang, W. Feng, C. Xu and Z. Wei, *J. Energy Chem.*, 2023, **81**, 167-191.
 201. Y. Xu, R. Ge, J. Yang, J. Li, S. Li, Y. Li, J. Zhang, J. Feng, B. Liu and W. Li, *J. Energy Chem.*, 2022, **74**, 45-71.
 202. C. Wang, L. Yu, F. Yang and L. Feng, *J. Energy Chem.*, 2023, **87**, 144-152.
 203. H. J. Son, M. J. Kim and S. H. Ahn, *Chem. Eng. J.*, 2021, **414**, 128739.
 204. K. Miao, J. Qin, J. Yang and X. Kang, *Adv. Funct. Mater.*, 2024, 2316824.
 205. X. Wang, X. Sang, C.-L. Dong, S. Yao, L. Shuai, J. Lu, B. Yang, Z. Li, L. Lei, M. Qiu, L. Dai and Y. Hou, *Angewandte Chemie*, 2021, **133**, 12066-12072.
 206. Y. Ma, T. Yang, H. Zou, W. Zang, Z. Kou, L. Mao, Y. Feng, L. Shen, S. J. Pennycook and L. Duan, *Adv. Mater.*, 2020, **32**, 2002177.
 207. Z. Nie, L. Zhang, X. Ding, M. Cong, F. Xu, L. Ma, M. Guo, M. Li and L. Zhang, *Adv. Mater.*, 2022, **34**, 2108180.
 208. Q. Shen, H. Jin, P. Li, X. Yu, L. Zheng, W. Song and C. Cao, *Nano Res.*, 2022, **15**, 5024-5031.
 209. L. Kuai, Z. Chen, S. Liu, E. Kan, N. Yu, Y. Ren, C. Fang, X. Li, Y. Li and B. Geng, *Nat. Commun.*, 2020, **11**.
 210. T. Wang, X. Tao, X. Li, K. Zhang, S. Liu and B. Li, *Small*, 2021, **17**, 2006255.
 211. B.-B. Xu, X.-B. Fu, X.-M. You, E. Zhao, F.-F. Li, Z. Chen, Y.-X. Li, X. L. Wang and Y.-F. Yao, *ACS Catal.*, 2022, **12**, 6958-6967.
 212. C. Hu, J. Hu, Z. Zhu, Y. Lu, S. Chu, T. Ma, Y. Zhang and H. Huang, *Angew. Chem. Int. Ed. Engl.*, 2022, **61**, e202212397.
 213. S. Tosoni, G. Di Liberto, I. Matanovic and G. Pacchioni, *J. Power Sources*, 2023, **556**, 232492.